remote sensing

MDPI

Article

Spire RO Thermal Profiles for Climate Studies: Initial Comparisons of the Measurements from Spire, NOAA-20 ATMS, Radiosonde, and COSMIC-2

Xin Jing [1,*], Shu-Peng Ho [2], Xi Shao [1], Tung-Chang Liu [1], Yong Chen [2] and Xinjia Zhou [3]

[1] Cooperative Institute for Satellite Earth System Studies (CISESS), Earth System Science Interdisciplinary Center, University of Maryland, College Park, MD 20740, USA; xshao@umd.edu (X.S.); tcliu@umd.edu (T.-C.L.)
[2] NOAA National Environmental Satellite, Data, and Information Service, Center for Satellite Applications and Research, College Park, MD 20740, USA; shu-peng.ho@noaa.gov (S.-P.H.); yong.chen@noaa.gov (Y.C.)
[3] Global Science & Technology, Inc., 7801 Greenway Center Drive, Suite 1100, Greenbelt, MD 20770, USA; xinjia.zhou@noaa.gov
* Correspondence: xinjing@umd.edu

Abstract: Global Navigation Satellite System (GNSS) Radio Occultation (RO) data play an essential role in improving numerical weather prediction (NWP) and monitoring climate change. The NOAA Commercial RO Purchase Program (CDP) purchased RO data provided by Spire Global Inc. To ensure the data quality from Spire Global Inc. is consistent with other RO missions, we need to quantify their accuracy and retrieval uncertainty carefully. In this work, Spire Wet Profile (wet temperature profile) data from 7 September 2021 to 31 October 2022, processed by the University Corporation for Atmospheric Research (UCAR), and COSMIC-2 (Constellation Observing System for Meteorology, Ionosphere, and Climate-2/Formosa Satellite Mission 7) data are evaluated through comparison with NOAA-20 Advanced Technology Microwave Sounder (ATMS) microwave sounder measurements and collocated RS41 radiosonde measurements. Through the Community Radiative Transfer Model (CRTM) simulation, we convert the Spire and COSMIC-2 RO retrievals to ATMS brightness temperature (BT) at sounding channels CH07 to CH14 (temperature channels), with weighting function peak heights from 8 km to 35 km, and CH19 to CH22 (water vapor channels), with weighting function peak heights ranging from 3.2 km to 6.7 km, and compare the simulations with the collocated NOAA-20 ATMS measurements over ocean. Using ATMS observations as references, Spire and COSMIC-2 BTs agree well with ATMS within 0.07 K for CH07-14 and 0.20 K for CH19-22. The trends between Spire and COSMIC-2 are consistent within 0.07 K/year over the oceans for ATMS CH07-CH13 and CH19-22, indicating that Spire/COSMIC-2 wet profiles are, in general, compatible with each other over oceans. The RO retrievals and RS41 radiosonde observation (RAOB) comparison shows that above 0.2 km altitude, RS41 RAOB matches Spire/COSMIC-2 temperature profiles well with a temperature difference of <0.13 K, and the trends between Spire and COSMIC-2 are consistent within 0.08 K/year over land, indicating that Spire/COSMIC-2 wet profiles are overall compatible with each other through RS41 RAOB measurements over land. In addition, the consistency of Spire and COSMIC-2 based on different latitude intervals, local times, and signal-to-noise ratios (SNRs) through ATMS was evaluated. The results show that the performance of Spire is comparable to COSMIC-2, even though COSMIC-2 has a higher SNR. The high quality of RO profiles from Spire is expected to improve short- and medium-range global numerical weather predictions and help construct consistent climate temperature records.

Keywords: radio occultation; spire; COSMIC-2; NOAA-20 ATMS; radiosonde; inter-comparison

Citation: Jing, X.; Ho, S.-P.; Shao, X.; Liu, T.-C.; Chen, Y.; Zhou, X. Spire RO Thermal Profiles for Climate Studies: Initial Comparisons of the Measurements from Spire, NOAA-20 ATMS, Radiosonde, and COSMIC-2. *Remote Sens.* **2023**, *15*, 3710. https://doi.org/10.3390/rs15153710

Academic Editor: Beatriz M. Funatsu

Received: 2 June 2023
Revised: 18 July 2023
Accepted: 19 July 2023
Published: 25 July 2023

1. Introduction

Global Navigation Satellite System (GNSS) Radio Occultation (RO) is a satellite remote sensing technique that uses GNSS receivers manifested on low-Earth orbit (LEO)

satellites to sense the occulted signals between GNSS emitters and receivers. The highly accurate and stable GNSS RO data are ideally suited for improving weather prediction, studying atmospheric processes, and monitoring climate [1–5]. The measurements obtained from the GNSS RO limb-sounding technique are free of mission-dependent and geographical-dependent biases [1,2]. The RO observations have the advantage of near-global coverage, all-weather capability, and high vertical resolution ranging from ~60 m near the surface to ~1.5 km at 40 km altitude [2–6]. The precision of RO temperature can reach ~0.1 K [7,8], and the precision of the trend of RO-derived temperature profiles is within ±0.06 K/5 years [9,10].

The National Oceanic and Atmospheric Administration (NOAA) Center for Satellite Applications and Research (STAR) is now processing GNSS RO data using independently developed inversion packages [11–13]. Using proper RO inversion procedures [11], we can convert the observed time delay to the excess phase profiles, which can be further converted into bending angle and refractivity profiles. The refractivity profile in the neutral atmosphere is a function of pressure, temperature, and moisture. To establish the NOAA long-term RO program and routinely monitor the RO data quality, NESDIS STAR has become an RO data processing and science center. This science center facilitates the following functions: (i) processing RO data [11,13–15], (ii) monitoring RO data quality, (iii) using RO data as an on-orbit reference to calibrate infrared and microwave measurements [16,17], (iv) optimizing RO data impacts on numerical weather prediction (NWP) [18,19], and (v) constructing climate data records (CDRs) and using RO data products to detect global change signals [13].

Currently, NOAA includes RO data from multiple RO missions in its numerical weather prediction (NWP) system (see Figure 1). The RO data assimilated into the current NOAA NWP system include the NOAA backbone mission (i.e., Constellation Observing System for Meteorology, Ionosphere, and Climate-2/Formosa Satellite Mission 7, hereafter COSMIC-2), Sentinel-6, and partners' missions (i.e., Challenging Minisatellite Payload Korea Multi-Purpose Satellite-5 (KOMPSAT-5) and Meteorological Operational satellite (MetOp) series -A/-B/-C GNSS Receiver for Atmospheric Sounding (GRAS)). While all these RO missions provide around 9 K–11 K occultation profiles per day (see Figure 1), the International Radio Occultation Working Group (IROWG) from the World Meteorology Organization (WMO) recommends that the optimal occultation number is at least 20 K per day with a uniform spatial and temporal distribution.

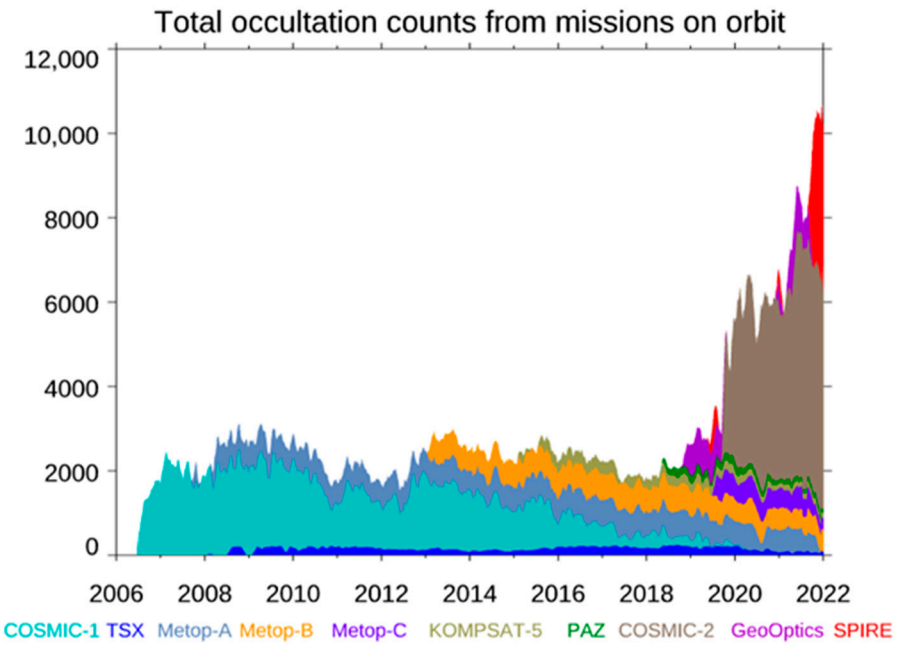

Figure 1. The total occultation counts from different missions in orbit.

Except for the nationally supported RO missions listed above, RO data can also be provided by commercial companies. To obtain more RO data and ensure the optimal spatial and temporal RO distribution from multiple RO missions, which best benefit the National Centers for Environmental Prediction (NCEP) global NWP, NOAA has established the Commercial Data Program (CDP) to facilitate RO data purchase. Spire Global Inc. and GeoOptics Inc. are the primary vendors to submit their data for CDP data assessment. Unlike COSMIC-2 and other nationally supported large RO satellite missions, GeoOptics and Spire RO data are collected from CubeSats. We can expect to reduce costs and shorten the extensive space mission/systems development procedures using CubeSat. The CubeSats usually have a smaller antenna size (e.g., ~1 foot for Spire) than nationally supported RO missions (e.g., 2 feet for COSMIC-2). As a result, the signal-to-noise ratio (SNR) for CubeSat may be smaller than other RO missions (see below). Spire currently operates a constellation of more than 110 CubeSats in LEO orbits, which collect about 20 K occultation profiles per day. The Spire Stratos RO antenna receiver payload can track GNSS signals from GPS, GLONASS (GLObal NAvigation Satellite System), Galileo, and QZSS (Quasi-Zenith Satellite System). Like COSMIC-2′s TriG (Global Positioning System—GPS, GALILEO, and GLONASS) GNSS RO Receiver System (TGRS), the GeoOptics's Community Initiative for Cellular Earth Remote Observation (CICERO) receiver can also track signals from GPS, GALILEO, and GLONASS.

Using the STAR RO processing and quality assessment system, we can assess the RO data quality purchased by the NOAA CDP. Spire Global Inc. (from now on referred to as Spire) is a commercial company that participated in the NOAA CDP RO data evaluation and purchasing. The company builds and operates more than 110 3U CubeSats low-Earth multi-use receivers (LEMURs). The LEMUR CubeSats fly in several sun-synchronous orbits at LEO satellites with altitudes ranging from 385 km to 650 km. Many publications and reports evaluated the accuracy of its bending angle [20,21], refractivity [20,22], SNR [20], occultation coverage [23,24], Ionospheric electron density measurements [25], and the detection of the planetary boundary layer height (PBLH) [26]. Alessandro Piro [27] from the European Space Agency evaluated one-month Spire temperature data (from 26 May 2019 to 25 June 2019) using collocated radiosonde data from the Integrated Global Radiosonde Archive (IGRA). They found that in the core region in the lower stratosphere, Spire temperature (i.e., dry temperature) data are highly consistent with those from IGRA radiosondes. However, for a specific range of altitudes, the data are not always comparable: 0–5 km, in particular close to 5 km (where moisture is significant); 12–13 km (Tropopause); and 35–40 km (Upper Stratosphere) [27].

Observations from GNSS RO, microwave sounders such as the Advanced Technology Microwave Sounder (ATMS), and radiosonde are all assimilated into the NCEP's NWP system. They are also used for climate studies [16,28–31]. Assessing the consistency and uncertainty among these data is critical in improving global weather predictions and helping to build a consistent climate temperature record [16,28,30,31].

This study assesses the inter-consistency between Spire and COSMIC-2 RO temperature profiles in the neutral atmosphere and those from ATMS measurements and radiosonde data. The Spire and COSMIC-2 Wet temperature profile data from 7 September 2021 to 31 October 2022 processed by the University Corporation for Atmospheric Research (UCAR) are used in this study. We estimated the temperature and trend differences between Spire and COSMIC-2 RO and compared them with NOAA-20 ATMS and collocated RS41 radiosonde measurements. The consistency between Spire and COSMIC-2 through ATMS and radiosonde are also evaluated. Through the Community Radiative Transfer Model (CRTM) simulations with RO retrievals as input, the brightness temperature (BT) from the NOAA-20 ATMS is compared with RO-simulated BTs for the ATMS CH07 to CH14 and CH19 to CH22 sounding channels over the ocean. The RS41 radiosonde temperature product collected from NCEP is used to evaluate the temperature and the trend differences between ROs and radiosonde data over land, from heights of 0.2 km to 35 km (corresponding to the weighting function peak height from the ATMS channels of interest).

The agreement between the Spire and COSMIC-2 data through radiosonde data via the double difference method is also estimated. In addition, we also quantify the difference between Spire and COSMIC-2 data for different latitudes, local times, and SNR groups through ATMS.

The paper is organized as follows. The datasets used in this work are described in Section 2. Section 3 describes the methodology. Section 4 presents the BT/Temperature (T) differences between two RO (i.e., Spire and COSMIC-2) products and ATMS/radiosonde over ocean and land, respectively. Section 4 also summarizes the trend between two RO products and ATMS over the ocean and analyzes the consistency of Spire and COSMIC-2 through the double difference method for different latitude intervals, local times, and SNRs. Section 5 provides discussions and summaries of the study.

2. Datasets

This section introduces the datasets used in this study and their related characteristics.

2.1. Radio Occultation Data

2.1.1. Spire

Each Spire LEMUR carries a GNSS Radio Occultation meteorology payload and a payload for ship tracking. The Spire GNSS payload is for atmosphere remote sensing and precision orbit determination. It uses occultation measurements to determine Earth's atmosphere temperature, pressure, and humidity profiles for applications in operational meteorology [32]. The Spire satellites are placed in low-Earth orbit (generally around 500 km altitude so that they naturally de-orbit) at various inclinations, including equatorial, sun-synchronous, and inclinations in between, allowing them to cover the globe. There are 35 satellites in the Spire constellation over the study period, and the number of satellites continues to grow. Spire RO data were provided to NOAA under the Commercial Weather Data for RO (CWD-RO) project. This work evaluates the Spire Wet Profile (wet temperature profiles) data from 7 September 2021 to 31 October 2022 processed by UCAR (https://data.cosmic.ucar.edu/gnss-ro/spire, accessed on 20 July 2023). The daily Spire occultation profiles purchased by CWD gradually increased from approximately 1000 on 7 September 2021 to about 4000 and then to around 6000 per day since 16 March 2022 (Figure 2). To facilitate comparisons with the Spire data, all other data used in this paper are from the same period.

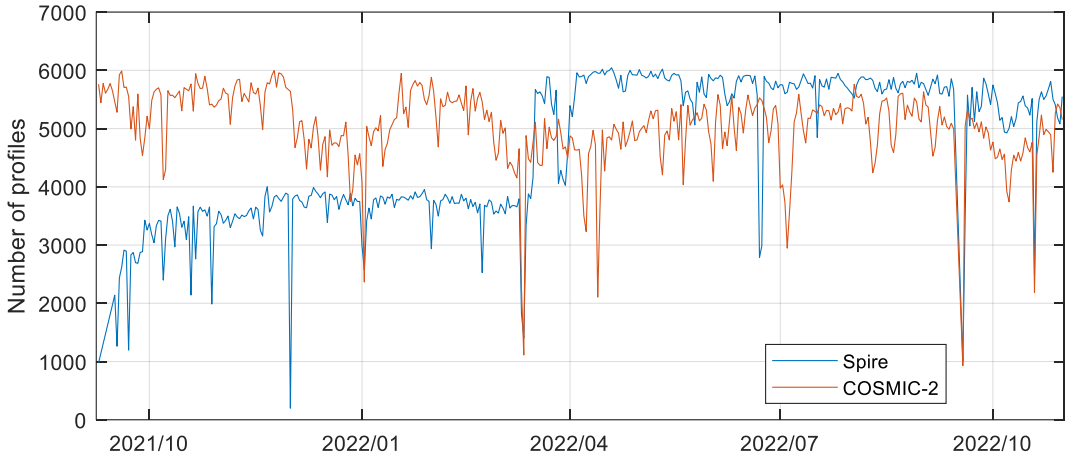

Figure 2. The processed number of RO profiles of SPIRE and COSMIC-2.

2.1.2. COSMIC-2

Launched on 15 April 2006, the Constellation Observing System for Meteorology, Ionosphere, and Climate-1/Formosa Satellite Mission 3 (COSMIC-1) has six satellites. COSMIC-1 has provided around 2000 to 3000 occultation profiles per day via the six receivers. As of mid-2019, COSMIC-1 still provides nearly 300 occultation profiles per day [32]. Launched

on 25 June 2019, COSMIC-2 is a COSMIC-1 follow-up mission. COSMIC-2 provides at least 4000 RO soundings daily, distributed between 45°N to 45°S. The inclination angle of its six identical microsatellites is 24°.

The UCAR developed one-dimension variational (1DVAR) retrieval algorithms to retrieve temperature and humidity profiles from COSMIC-2 and Spire RO refractivity profiles [16]. UCAR Spire and COSMIC-2 converted a priori values from GFS forecasts to the European Centre for Medium-Range Weather Forecasts (ECMWF) 6 h interval forecasts on 27 October 2021 and 8 September 2021, respectively. The retrieved product, the UCAR wetPf2 soundings generated at near real-time (NRT), was released in October 2019 and made publicly available on the web at https://data.cosmic.ucar.edu/gnss-ro/COSMIC-2/nrt/ (accessed on 3 June 2022). WETPf2 data provide temperature and water vapor profiles up to 60 km altitude with a 0.05 km vertical resolution from mean sea level height up to 20 km and 0.1 km from 20 km to 60 km. As shown in Figure 2, the COSMIC-2 data profile processed by UCAR remained stable between 4000 and 6000 per day from 7 September 2021 to 31 October 2022.

In this study, we used validated COSMIC-2 data to assess the quality of Spire data products. The accuracy of COSMIC-2-derived temperature profiles is better than 0.5 K from 8 km to 30 km [16,33]. The trend stability between simulated BTs using COSMIC-2 retrievals and ATMS measurements is <0.02 K/year for ATMS CH07–10. The BT trend difference for ATMS CH19–21 is <0.06 K/year [16,34].

2.2. NOAA-20/ATMS

The Advanced Technology Microwave Sounder (ATMS) built by Northrop Grumman, Azusa, CA, USA, is the latest operational microwave sounder series launched by the United States to provide both temperature and water vapor soundings of the atmosphere. The first ATMS on the Suomi National Polar-orbiting Partnership (SNPP) satellite was launched in 2011. The second ATMS was launched in November 2017 on the Joint Polar Satellite System-1 satellite (JPSS-1) and was renamed NOAA-20. It joins the first ATMS flight unit aboard the SNPP satellite and older sounders—i.e., the Advanced Microwave Sounding Units A and B (AMSU-A/B) and Microwave Humidity Sounder (MHS)—on polar-orbiting operational weather satellites. These sounders provide critical all-weather temperature and humidity profile information for NWP models. SNPP is in a sun-synchronous orbit [35,36], with an altitude of 824 km and an inclination of 97.1, yielding an orbital period of 101 min, with the ascending equatorial crossing time set at 01:30 P.M. local time. NOAA-20, whose nominal equator crossing local time and altitude are the same as SNPP, flies about 50 min ahead of SNPP, allowing important overlap in the observational coverage.

The ATMS has 22 channels spanning 23-183 GHz, closely following the channel set of the legacy microwave instruments such as Microwave Sounding Unit (MSU), AMSU-A, AMSU-B, MHS, and Humidity Sounder for Brazil (HSB). The ATMS product used in this work is the Sensor Data Record (SDR). The SDR provides Level 1b calibrated and geolocated radiance/BT data for measuring atmospheric temperature and moisture. NOAA-20 ATMS SDR data in this study were obtained from the NOAA Comprehensive Large Array-Data Stewardship System (CLASS, https://www.avl.class.noaa.gov/saa/products/welcome, accessed on 20 July 2023).

Figure 3 shows the weighting functions for ATMS CH07-14 and CH19-22, demonstrating the sensitivity of atmospheric absorption and radiation contribution at different altitudes to the observed ATMS channel BTs. These ATMS channel weighting functions were calculated using the CRTM for the U.S. standard atmosphere at the nadir and over a water surface. It can be seen that the peak heights of the water vapor sounding CH19-22 are below 7 km and can reach as low as around 3 km for channel 19. The peak heights of temperature sounding CH07-14 range from 8 to 35 km. Because RO retrievals may have a larger uncertainty above 35 km and below 2 km, the ATMS soundings CH07-14 and CH19-22 are selected in this study.

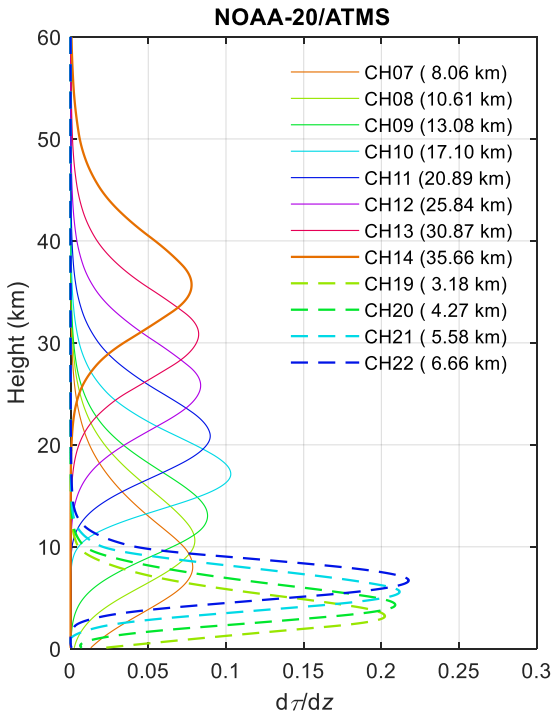

Figure 3. The weighting functions of NOAA-20/ATMS channels used in this work were generated using the U.S. standard atmosphere over water surface input into the Community Radiative Transfer Model (CRTM).

2.3. Radiosonde Data

While NOAA-20 ATMS was used to evaluate the temperature of RO data consistency over the oceans, we estimated the RO temperature accuracy over land using radiosonde data. The radiosonde network is one of the reliable data sources, providing the longest humidity record in the troposphere and lower stratosphere. Radiosonde observations have also been used as a benchmark to validate satellite-retrieved sounding products [37]. The radiosonde profiles used in this work were extracted from the NCEP Automated Data Processing (ADP) Global Upper Air Observational Weather Data (dataset ds351.0). The data include pressure, geopotential height, air temperature, dew point temperature, wind direction, and speed. The radiosonde data are available at up to 20 mandatory levels from 1000 millibars to 1 millibar, plus a few significant levels. Data intervals range from hourly to 12 h. The data format is WMO BUFR (http://rda.ucar.edu/#BUFR, accessed on 20 July 2023). We used the NCEP BUFRLIB software version 1.0 (https://github.com/NOAA-EMC/NCEPLIBS-bufr/, accessed on 20 July 2023) to decode BUFR messages and extract the radiosonde profiles. All the BUFR data were downloaded from the Computational and Information Systems Laboratory (CISL) Research Data Archive (http://rda.ucar.edu/datasets/ds351.0/, accessed on 20 July 2023). Vaisala RS92 was one of the major sonde types in the global operational upper air network but has gradually been replaced by Vaisala RS41 starting in late 2013. The sensor technologies and state-of-the-art design and manufacturing methodologies of the RS41, combined with its extreme ease of use, ensure reliable and highly accurate atmospheric observations [38]. We only use RS41 measurements in this study.

2.4. ERA5

ERA5 is the fifth generation ECMWF atmospheric reanalysis of the global climate covering the period from January 1950 to the present. ERA5 is produced by the Copernicus Climate Change Service (C3S) at ECMWF. ERA5 provides hourly estimates for atmospheric, ocean-wave, and land-surface quantities, with $0.25^\circ \times 0.25^\circ$ horizontal resolution. The data cover the globe and resolves the atmosphere using 137 levels from the surface up to 80 km (0.01 hPa). Atmospheric data used in this work are interpolated to 37 pressures. This

paper used RO temperature, water vapor, and ERA5 surface products, including surface temperature, wind, and ozone on pressure levels, as input to the CRTM radiative transfer model to simulate ATMS brightness temperatures.

3. Methodology

Figure 4 summarizes the methodology and processes used in this paper to evaluate the consistency between Spire and COSMIC-2 data. The main idea of this paper is to use both NOAA-20 ATMS and radiosonde observations as the references and compare them with Spire and COSMIC-2 data, and then through NOAA-20 ATMS and radiosonde data, Spire and COSMIC-2 can be compared via the double difference method. Since the land and ocean surface emissivity is very different, to minimize the uncertainty of the reference data, NOAA-20 ATMS is only used as the reference data for the ocean region in this paper. To compare with the brightness temperature data provided by NOAA-20 ATMS, a radiometric simulation using the CRTM was needed to obtain the RO-simulated brightness temperature using RO temperature and humidity data and ERA5 atmospheric and surface parameters as inputs. The temperature difference and its trend over the land region were validated with radiosonde observations. The sensitivity to SNR, latitude, and local time was further analyzed to understand the effect of the different instrumental specifications of Spire and COSMIC-2 on the results. Detailed information on each step is described in the following subsections.

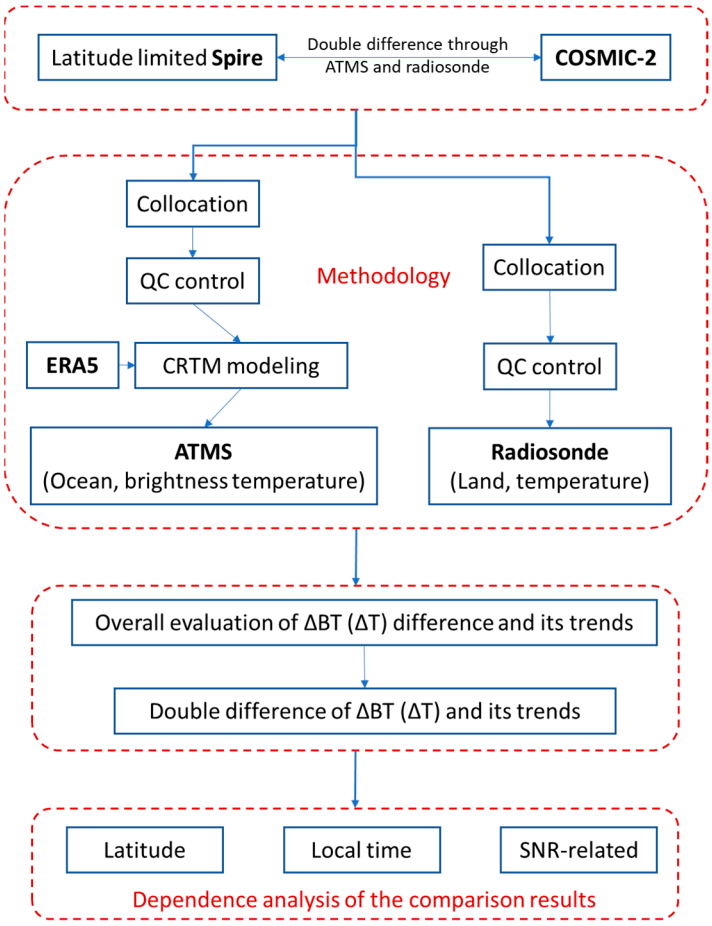

Figure 4. Flow chart of the procedure to evaluate the consistency between Spire and COSMIC-2 through ATMS and radiosonde data.

3.1. Latitude Limitations

The geographical coverage of RO measurements is an important feature that affects RO performance. The spatial coverage of Spire can complement the six operational COSMIC-2

satellites. Figure 5 shows the percentage of latitudinal distribution of occultation events for Spire (blue) and COSMIC-2 (red) between 7 September 2021 and 31 October 2022. The latitudinal distributions demonstrated that Spire data, characterized by various inclination orbits (51.6°, 83°/85°, and 37°), resulted in observations concentrated more in the mid-latitudes. On the other hand, due to the low orbital inclination of the satellite (24°), the RO events of COSMIC-2 cover only latitudes within ±45°, and many events are concentrated at low latitudes. In this work, only RO events from the same latitudinal region (45°S to 45°N) observed by Spire and COSMIC-2 were included in the calculation and evaluation. The other data used in this paper also limited the latitude to ±45°.

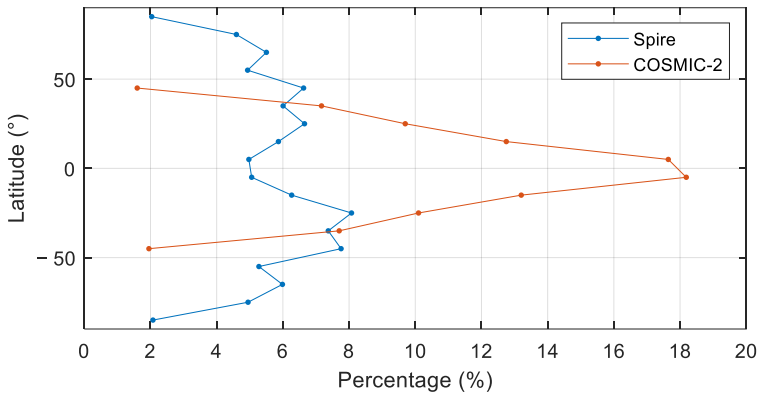

Figure 5. Percentage of latitudinal distribution of occultation events for Spire and COSMIC-2 between 7 September 2021 and 31 October 2022.

3.2. Collocation, Quality Control, and Interpolation

In studying the intercomparison of RO and reference data, screening and matching the relevant data measured by both is necessary. In this study, the collocated RO and reference data are first collected over the area of interest, within (45°S and 45°N) latitude over oceans for ATMS and over land for radiosonde. Figure 6 shows the collocation between Spire (left)/COSMIC-2 (right) and NOAA-20 ATMS over the ocean. It can be seen that a number of the collocations of Spire and ATMS do fall outside the 45°S to 45°N latitude range, so it is necessary to limit the latitude range of the Spire-ATMS collocation. The matching criteria were set to a time difference of no more than 2 h and a spatial distance of no more than 150 km [16,31]. The spatial difference is defined as the difference between the perigee point location of the RO profile and the NOAA-20 ATMS nadir. Such matching criteria ensure that the RO and ATMS/radiosonde observed a reasonably similar atmospheric state. Table 1 shows the number of collocated RO profiles over land and oceans. The number of Spire profiles paired with ATMS and radiosonde was reduced by 67% and 31%, respectively, after latitude was limited. The significant decrease in ATMS collocation is mainly due to the large concentration of ATMS data in the north and south polar regions.

In addition, only good RO profiles, which have attribute flags "bad" = 0 and "L2P" $\neq$ "P", are considered in the collocation process. The "bad" flag indicates that the COSMIC-2 retrieval results are of low quality and should be excluded from the analysis. The "L2P" flag refers to an ascending COSMIC-2 occultation that uses a GNSS transmitter and L2P carrier frequency. In the provisional version of COSMIC-2 data, there is a bias in the processing of L2P data. Therefore, this analysis does not include COSMIC-2 data with the "L2P" flag. The matching criteria are applied throughout the study period. It is important to note that these quality control attributes are only applied to COSMIC-2 since Spire does not have them. It can be seen from Table 1 that around 12% and 18% of COSMIC-2 collocated with ATMS and radiosonde profiles, respectively, were screened out using QC attributes.

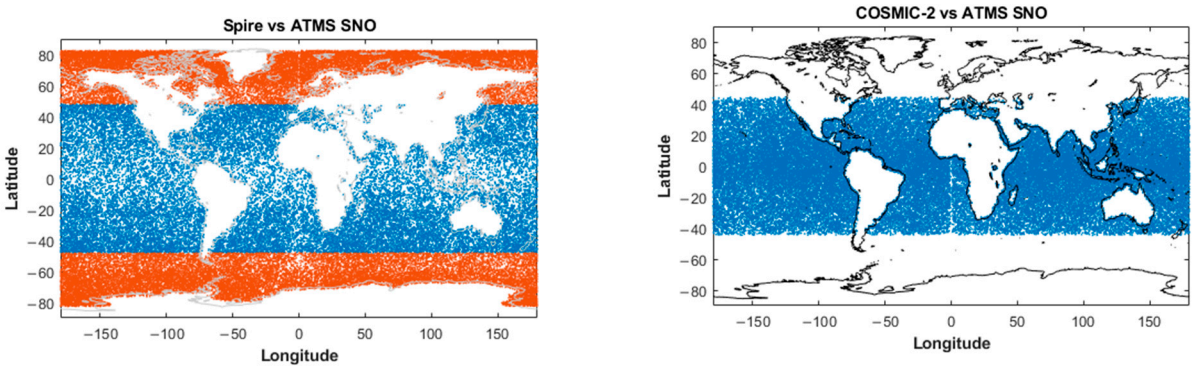

Figure 6. The collocation between Spire (**left**)/COSMIC-2 (**right**) and NOAA-20 ATMS. The red and blue dots in the left figure indicate the collocation outside and within (45°S and 45°N) latitude, respectively.

Table 1. The number of collocated RO profiles for each preprocessing step.

Matching Pairs	ATMS (Ocean)		Radiosonde RS41 (Land)	
	Spire	COSMIC-2	Spire	COSMIC-2
Original	1,499,067	1,038,827	14,825	12,441
Latitude	445,373	1,038,827	10,190	12,441
QC	445,373	911,560	10,190	10,971
Ocean/land	346,987	691,032	6494	7237
Outlier	345,553~346,967 (CH7-14) 252,184~280,608 (CH19-22)	686,989~691,021 (CH7-14) 521,247~565,018 (CH19-22)	See Figure 8b	See Figure 8b

Inevitably, there will be some outliers when the two data types are compared. Therefore, for ATMS, values with a brightness temperature difference between the observation and the CRTM simulation greater than 5 K were considered outliers. Similarly, for the radiosonde data, each pressure layer with a temperature difference greater than 5 K from the RO was marked as an outlier. Table 1 shows that the number of Spire and COSMIC-2 profiles paired with ATMS was reduced by 0.05% and 0.5% for CH07-14, respectively, and by no more than 27% and 25% for CH19-22, respectively. The outliers in channels CH19-22 are mainly from the influence of cloud cover. Since the number of the paired profiles with radiosonde are different at each pressure level, the remaining number of paired profiles with radiosonde is not shown in Table 1 but can be found in Figure 8b.

The datasets used in this work had different vertical resolutions. To minimize the mismatch of vertical resolutions, RO temperature, and ECMWF atmosphere profiles were all linearly interpolated (in the logarithmic pressure coordinate) to the ECMWF L60 model level. Then, they were passed to the CRTM model to calculate the ATMS brightness temperatures.

3.3. CRTM

The Community Radiative Transfer Model (CRTM) is developed by the U.S. Joint Center for Satellite Data Assimilation (JCSDA) for rapid satellite radiance simulations and radiance derivative calculations under various atmospheric and surface conditions [17,39–41]. CRTM supports many sensors covering the microwave, infrared, and visible frequency regions, including the historical and near-future sensors from the Geostationary Operational Environmental Satellite-R (GOES-R) and JPSS. This study used CRTM (v2.1.3) for forward modeling to simulate the BT of ATMS channels using RO temperature profiles. To simulate the BT of ATMS channels, the temperature and water vapor profiles from RO data were fed as inputs to the CRTM. Other inputs to the CRTM simulation include surface

parameters such as skin temperature, wind speed, wind direction, and ozone atmosphere profile, which were obtained from ERA5 based on six-hour increments.

4. Results

This study used the difference between simulated BT from RO soundings and observed BT from ATMS (ΔBT) and the ΔBT drift during the selected period to evaluate the RO temperature products' consistency and stability over the ocean. Similarly, the difference between RO and radiosonde temperature (ΔT) and its drift over time was used to evaluate similar RO sounding fidelity over land.

4.1. Overall Evaluation of ΔBT (ΔT) and Its Trends over Ocean (Land)

4.1.1. ΔBT and ΔT Evaluation

The section compares the CRTM-simulated BT data using RO wet temperature profiles from Spire and COSMIC-2 data products over the ocean as inputs with NOAA-20/ATMS measurements. In addition, the T profiles from Spire and COSMIC-2 data products over the land were compared with radiosonde RS41 measurements.

Figure 7a shows the mean BT difference $\mu(\Delta BT_{RO\_ATMS})$. Uncertainty (i.e., $\sigma(\Delta BT_{RO_{ATMS}})$) of the mean TB difference between the RO-simulated BT and NOAA-20/ATMS observation over the ocean and the associated results are listed in Table 2. In this paper, uncertainty is defined as the 1-sigma standard deviation of the data. Figure 7 (a) shows that both the mean BT difference for Spire ($\mu(\Delta BT_{Spire\_ATMS})$) and COSMIC-2 ($\mu(\Delta BT_{C2\_ATMS})$ and their corresponding uncertainty for Spire (i.e., $\sigma(\Delta BT_{Spire\_ATMS})$ and COSMIC-2 ($\sigma(\Delta BT_{C2\_ATMS})$ are consistent in both the magnitude and sign for all ATMS channels of interest. In particular, the $\mu(\Delta BT_{Spire\_ATMS})$ and $\mu(\Delta BT_{C2\_ATMS})$ are all within 0.63 K for the ATMS channels of interest except for CH09, with which $\mu(\Delta BT_{Spire\_ATMS})$ and $\mu(\Delta BT_{C2\_ATMS})$ remain less than 1 K. This is consistent with previous work from Shao et al. [16]. Since the $\mu(\Delta BT_{Spire\_ATMS})$ and $\mu(\Delta BT_{C2\_ATMS})$ for ATMS CH09 are very close, which are 0.90 K and 0.94 K, respectively, it can be considered that the relatively significant BT difference with ATMS CH09 is due to the uncertainty of ATMS observation or CRTM simulation.

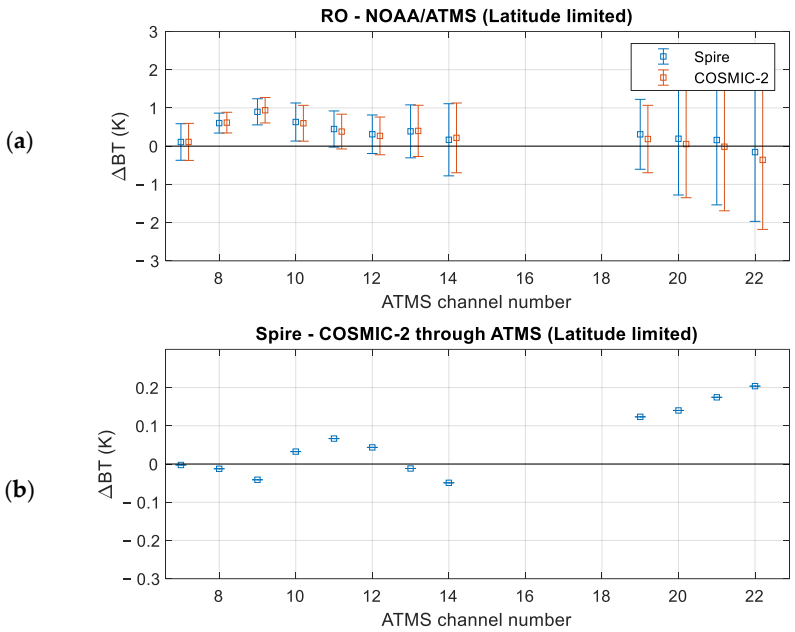

Figure 7. The BT difference between (**a**) NOAA/ATMS CRTM-simulated measurements using RO soundings and observations and (**b**) Spire and COSMIC-2 computed with the double difference method by using ATMS data over the ocean as a transfer reference. The vertical bar indicates the uncertainty in (**a**).

Table 2. (Left) The BT difference between NOAA/ATMS CRTM-simulated measurements using RO soundings and observations taken from Figure 7 and (right) the T difference between RO and radiosonde T taken from Figure 8.

RO vs. ATMS (K ± K)				RO vs. Radiosonde (K ± K)			
Channel (Peak Sounding Height, km)	**Spire**	**COSMIC-2**	**Spire–COSMIC-2**	**Height (km)**	**Spire**	**COSMIC-2**	**Spire–COSMIC-2**
7 (8.06)	0.11 ± 0.48	0.11 ± 0.48	0.00	0.2	0.41 ± 1.77	0.24 ± 1.68	0.17
8 (10.61)	0.60 ± 0.26	0.62 ± 0.27	−0.01	1.0	−0.02 ± 1.39	−0.13 ± 1.35	0.11
9 (13.08)	0.90 ± 0.34	0.94 ± 0.33	−0.04	2.0	−0.04 ± 1.23	−0.01 ± 1.17	−0.03
10 (17.10)	0.63 ± 0.50	0.60 ± 0.47	0.03	3.2	−0.02 ± 1.15	−0.00 ± 1.08	−0.01
11 (20.89)	0.45 ± 0.47	0.38 ± 0.45	0.07	4.2	0.05 ± 1.17	0.09 ± 1.08	−0.04
12 (25.84)	0.31 ± 0.50	0.27 ± 0.49	0.04	5.6	−0.02 ± 1.17	0.08 ± 1.12	−0.10
13 (30.87)	0.39 ± 0.69	0.40 ± 0.67	−0.01	6.6	0.03 ± 1.18	0.16 ± 1.15	−0.12
14 (35.66)	0.17 ± 0.94	0.22 ± 0.91	−0.05	8.0	0.08 ± 1.16	0.17 ± 1.10	−0.09
19 (3.18)	0.31 ± 0.91	0.19 ± 0.88	0.12	10.5	0.05 ± 1.04	0.12 ± 0.97	−0.07
20 (4.27)	0.19 ± 1.47	0.05 ± 1.40	0.14	13.0	0.01 ± 1.06	0.02 ± 0.96	−0.01
21 (5.58)	0.16 ± 1.70	−0.01 ± 1.68	0.17	17.0	0.02 ± 1.43	0.00 ± 1.44	0.02
22 (6.66)	−0.16 ± 1.81	−0.36 ± 1.82	0.20	21.0	−0.01 ± 1.34	−0.05 ± 1.36	0.04
				26.0	0.06 ± 1.46	−0.00 ± 1.44	0.06
				30.0	−0.13 ± 1.70	−0.04 ± 1.77	−0.09

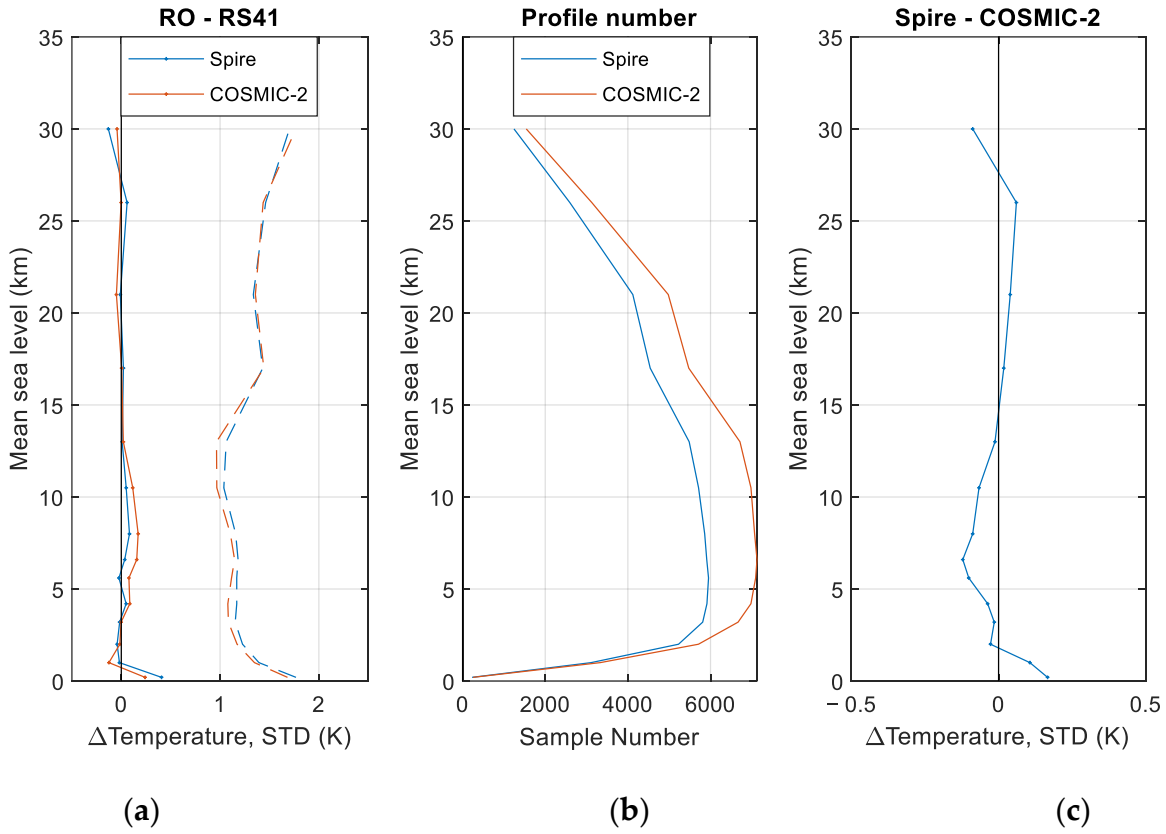

Figure 8. (**a**) The temperature difference between RO and radiosonde RS41 instrument measurements, (**b**) the sample number profile associated with the data in (**a**), and (**c**) the temperature difference between Spire and COSMIC-2 using the radiosonde data as a transfer standard in the double difference method.

Figure 7a depicts that the magnitudes of BT difference uncertainty are comparable between $\sigma(\Delta BT_{Spire\_ATMS})$ and $\sigma(\Delta BT_{C2\_ATMS})$. The values of $\sigma(\Delta BT_{Spire\_ATMS})$ and $\sigma(\Delta BT_{C2\_ATMS})$ for ATMS CH07 to CH12 are within 0.50 K, but are larger than 0.66 K for ATMS CH13 and 14, which have weighting function peak heights of 30.87 km and 35.66 km, respectively. Since the Radio Occultation bending angle decreases exponentially with

decreasing air density, the temperature uncertainty increases quickly above ~25 km [42,43]. This is why we found the larger BT uncertainty for ATMS CH13 and CH14. Uncertainty values greater than 0.66 K are also found for ATMS CH19-22, where weighting function peak heights range between 3.18 km and 6.66 km. This relatively large uncertainty in the tropospheric water vapor sounding channels—i.e., ATMS CH19-22—is possibly due to the large water vapor variation in the lower troposphere.

Figure 7b shows the mean BT difference between Spire and COSMIC-2 $\mu(\Delta BT_{Spire\_C2})$ computed with the double difference method using ATMS data over the ocean as a transfer reference. These results are also in Table 2. Note the magnitude of the total uncertainty $\sigma(\Delta BT_{Spire\_C2}) = \sqrt{(\sigma(\Delta BT_{Spire\_ATMS}))^2 + (\sigma(\Delta BT_{C2\_ATMS}))^2}$ is larger than the magnitude of $\sigma(\Delta BT_{Spire\_ATMS})$ and $\sigma(\Delta BT_{C2\_ATMS})$. To explicitly show the magnitude of the mean double difference between the two RO missions, we do not include the total uncertainty $\sigma(\Delta BT_{Spire\_C2})$ in Figure 7b. Figure 7b shows that Spire and COSMIC-2 CRTM-simulated BT agree well and are within 0.07 K for ATMS CH07-14. The BT differences for ATMS CH19-22 are relatively large but still not larger than 0.2 K. The double BT difference between Spire and COSMIC-2 $\mu(\Delta BT_{Spire\_C2})$ indicates that the performance of Spire and COSMIC-2 temperature and water vapor retrievals are very compatible from the surface to around 30 km altitude. The relatively large discrepancies below 7 km altitude may be due to the larger water vapor variation in the lower troposphere.

The NCEP radiosonde temperature product is used to evaluate the temperature consistency of Spire and COSMIC-2 over land. Since the radiosonde measures the vertical profile of pressure, temperature, and humidity from the ground to the balloon burst height limit of about 35 km, this paper takes advantage of its high accuracy of ground observation by adding three additional evaluations at heights of 0.2, 1, and 2 km to fill the gap in the accurate assessment between ATMS observations and simulations using RO retrievals. The RO and radiosonde comparison heights close to the weighting function peak height of ATMS channels of interest were selected to demonstrate the consistency between the two RO data sets over land using the radiosonde dataset.

Figure 8a,b show the mean $\mu(\Delta T_{RO\_raob})$ (solid lines in Figure 8a) and uncertainty $\sigma(\Delta T_{RO\_raob})$ (dash lines in Figure 8a) of the temperature difference between the RO and RS41 measurements and the sample number, at the heights of interest, respectively. Table 2 lists the results of Figure 8. In general, both the mean T difference in $\mu\left(\Delta T_{Spire\_raob}\right)$ and $\mu(\Delta T_{C2\_raob})$ and the temperature difference uncertainty in $\sigma\left(\Delta T_{Spire\_raob}\right)$ and $\sigma(\Delta T_{C2\_raob})$ are consistent in both the magnitude and sign for all heights of interest. In particular, the $\mu\left(\Delta T_{Spire\_raob}\right)$ and $\mu(\Delta T_{C2\_raob})$ are all within 0.17 K for the heights of interest except for 0.2 km altitude, with which the difference in Spire and COSMIC-2 remain within 0.41 K. As for the temperature difference uncertainty, the magnitudes of T difference uncertainty are very similar between $\sigma\left(\Delta T_{Spire\_raob}\right)$ and $\sigma(\Delta T_{C2\_raob})$, and their values are between ~1 K and ~2 K for all heights of interest.

The values for $\sigma\left(\Delta T_{Spire\_raob}\right)$ and $\sigma(\Delta T_{C2\_raob})$ for the heights 10.5 km and 13 km are relatively small, which is consistent with the $\sigma(\Delta BT_{Spire\_ATMS})$ and $\sigma(\Delta BT_{C2\_ATMS})$ for the ATMS CH08 and CH09, whose peak heights are 10.61 km and 13.08 km, respectively. In addition, similar to $\sigma(\Delta BT_{Spire\_ATMS})$ and $\sigma(\Delta BT_{C2\_ATMS})$, the larger T difference uncertainty is larger for heights higher than 25 km due to the Radio Occultation temperature retrieval uncertainty increasing with height above 25 km.

Figure 8c shows the mean temperature difference $\mu(\Delta T_{Spire\_C2})$ between Spire and COSMIC-2, using the radiosonde temperature as a transfer reference via the double difference method. The associated data values are given in Table 2. Similar to the BT double difference using ATMS as a reference, the total uncertainty $\sigma(\Delta T_{Spire\_C2})$ is propagated from the uncertainties of the T difference between ROs and radiosonde, i.e., $\sigma\left(\Delta T_{Spire\_raob}\right)$ and $\sigma(\Delta T_{C2\_raob})$. To clearly show the magnitude of the temperature double difference

between the two RO missions, the total uncertainty $\sigma(\Delta T_{Spire\_C2})$ is not shown in Figure 8c. Figure 8c depicts that Spire and COSMIC-2 temperatures agree within 0.17 K from 0.2 km to 30 km. The Spire temperature shows small negative differences over the height region between 2 km to 13 km and at the height of 30 km. This is similar to the BT double difference results using ATMS as a reference, which shows a slight negative difference in Spire at the ATMS channel weighting function peak height of ~10–~13 km and higher than 30 km.

The above results show that Spire and COSMIC-2 agree very well at different heights. Their BT and T differences through the double difference approach are all within 0.10 K, except for the ATMS four water vapor channels (CH19-22) and 0.2 km and 1.0 km height of RAOB comparison, whose BT differences are not larger than 0.20 K.

4.1.2. Trend Evaluation

Figure 9 shows the ΔBT_{RO_ATMS} time series plots and daily BT difference trend $D(\Delta BT_{RO\_ATMS})$ and its associated 95% confidence interval (CI) obtained from the F-test, between Spire/COSMIC-2 and NOAA-20 ATMS measurements for ATMS CH07-14 and CH19-22. To evaluate the time series potential BT difference trend between RO and ATMS, linear regressions of daily average BT difference vs. days were fitted to obtain lines of best fit, and the slopes of these fitted lines were used to calculate the yearly drift. Table 3 lists the data associated with these results. The most noticeable feature in Figure 9 is the larger scattering of the daily difference for the ATMS CH14 and CH19-22, which is consistent with the BT difference uncertainties $\sigma(\Delta BT_{RO\_ATMS})$ for these channels (see Table 2). Figure 9 also shows the discrepancy between ΔBT_{Spire_ATMS} and ΔBT_{C2_ATMS} in the first two months of the ATMS CH12 to CH14 (weighting function peak height > 25 km). This discrepancy in ATMS CH12-14 is mainly owing to the UCAR WETPf2 1D-Var algorithm updates, i.e., the UCAR Spire and COSMIC-2 change to ECMWF 6 h forecasts from GFS forecasts as a priori values around 27 October 2021 and on 8 September 2021, respectively. Since ECMWF relies strongly on the ATMS data, the RO data show stronger agreement with the ATMS data after the background data are updated.

Table 3. Values of the trend and associated 95% confidence interval for the differences between daily Spire/COSMIC-2 CRTM-simulated BT (sounding T) and NOAA-20 ATMS BT (RS41 radiosonde T) measurements from 8 September 2021 to 31 October 2022. These values are also given for the comparison of Spire and COSMIC-2 BT (T) trends formed using the double difference method with NOAA-20 ATMS (RS41 radiosonde) data as a transfer reference.

RO vs. ATMS (K/Year ± K/Year)				RO vs. Radiosonde (K/Year ± K/Year)			
Channel (Peak Sounding Height, km)	**Spire**	**COSMIC-2**	**Spire–COSMIC-2**	**Height (km)**	**Spire**	**COSMIC-2**	**Spire–COSMIC-2**
7 (8.06)	−0.02 ± 0.02	−0.03 ± 0.01	0.01	0.2	−0.03 ± 0.53	−0.19 ± 0.43	0.16
8 (10.61)	−0.01 ± 0.01	0.00 ± 0.01	−0.01	1.0	−0.03 ± 0.18	−0.19 ± 0.15	0.16
9 (13.08)	−0.01 ± 0.01	0.00 ± 0.01	−0.01	2.0	0.02 ± 0.12	0.03 ± 0.10	−0.01
10 (17.10)	0.03 ± 0.02	0.01 ± 0.01	0.02	3.2	0.12 ± 0.11	−0.00 ± 0.09	0.12
11 (20.89)	0.07 ± 0.02	0.05 ± 0.01	0.02	4.2	0.06 ± 0.11	0.09 ± 0.09	−0.02
12 (25.84)	0.08 ± 0.02	0.11 ± 0.02	−0.03	5.6	0.04 ± 0.11	0.02 ± 0.09	0.02
13 (30.87)	0.03 ± 0.03	0.10 ± 0.02	−0.07	6.6	0.01 ± 0.11	0.01 ± 0.09	0.00
14 (35.66)	−0.07 ± 0.04	0.05 ± 0.03	−0.12	8.0	−0.07 ± 0.11	0.04 ± 0.09	−0.11
19 (3.18)	−0.00 ± 0.03	0.01 ± 0.02	−0.01	10.5	−0.02 ± 0.11	−0.01 ± 0.08	−0.01
20 (4.27)	0.07 ± 0.06	0.01 ± 0.04	0.06	13.0	0.04 ± 0.10	0.02 ± 0.08	0.02
21 (5.58)	−0.01 ± 0.06	−0.00 ± 0.04	−0.01	17.0	0.08 ± 0.15	−0.00 ± 0.14	0.08
22 (6.66)	−0.08 ± 0.07	−0.02 ± 0.05	−0.06	21.0	0.12 ± 0.15	−0.01 ± 0.13	0.13
				26.0	−0.04 ± 0.19	−0.11 ± 0.17	0.07
				30.0	−0.26 ± 0.29	−0.28 ± 0.24	0.02

For the daily BT difference trend, $D(\Delta BT_{RO\_ATMS})$, Table 3 shows that both $D(\Delta BT_{Spire\_ATMS})$ and $D(\Delta BT_{C2\_ATMS})$ for all ATMS channels of interest are within ±0.11 K/year. As for the yearly drift difference between Spire and COSMIC-2, $\Delta D(\Delta BT_{Spire\_C2})$, created using the double difference with ATMS data as a transfer reference, the two RO-based CRTM-simulated BT trends agree with each other within 0.06 K/year. The ex-

ception is ATMS CH13 and CH14, which have trends that differ by −0.07 K/year and −0.12 K/year, respectively.

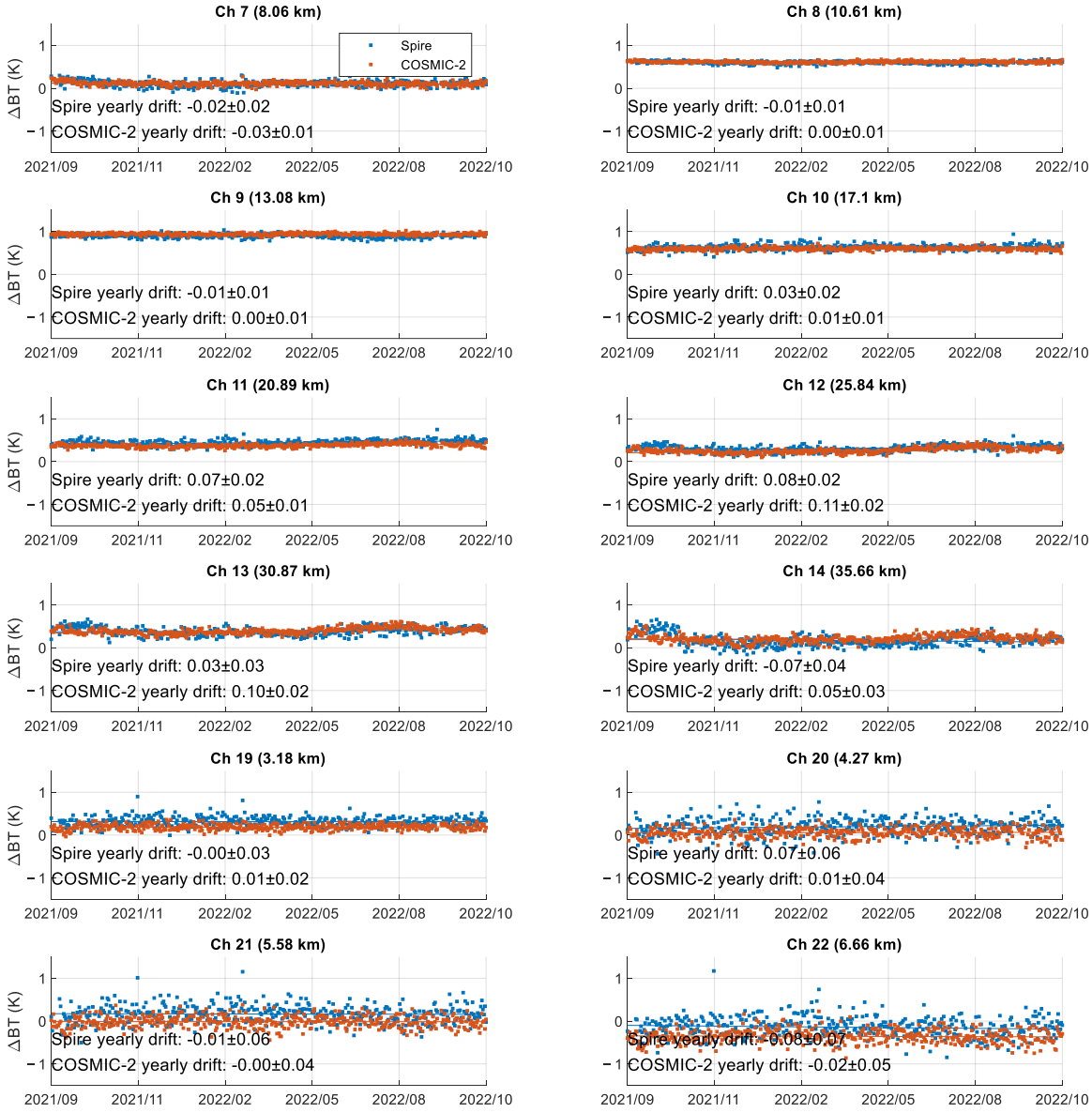

Figure 9. The time series and trend and its associated 95% confidence interval of daily BT differences between Spire/COSMIC-2 and NOAA-20 ATMS measurements from 8 September 2021 and 31 October 2021 for ATMS CH07-14 and CH19-22.

Figure 10 shows the daily ΔT_{RO_raob} time series plots and their trends, $D(\Delta T_{RO\_raob})$, and associated 95% CIs, between Spire/COSMIC-2 and radiosonde temperature measurements for 12 heights of interest. The results are also listed in Table 3. Given the large uncertainty and smaller number of data points at 0.2 km and 30 km (see Table 2 and Figure 7b), the time series and trends are not shown in Figure 10 for these two heights. Similar to the analysis of RO performance, based on the CRTM-simulated and observed ATMS BT difference trend comparisons, $D(\Delta T_{RO\_raob})$ for the surface heights and heights larger than 25 km have more scattering. This is also consistent with the T difference uncertainties $\sigma(\Delta T_{RO\_raob})$ for these heights.

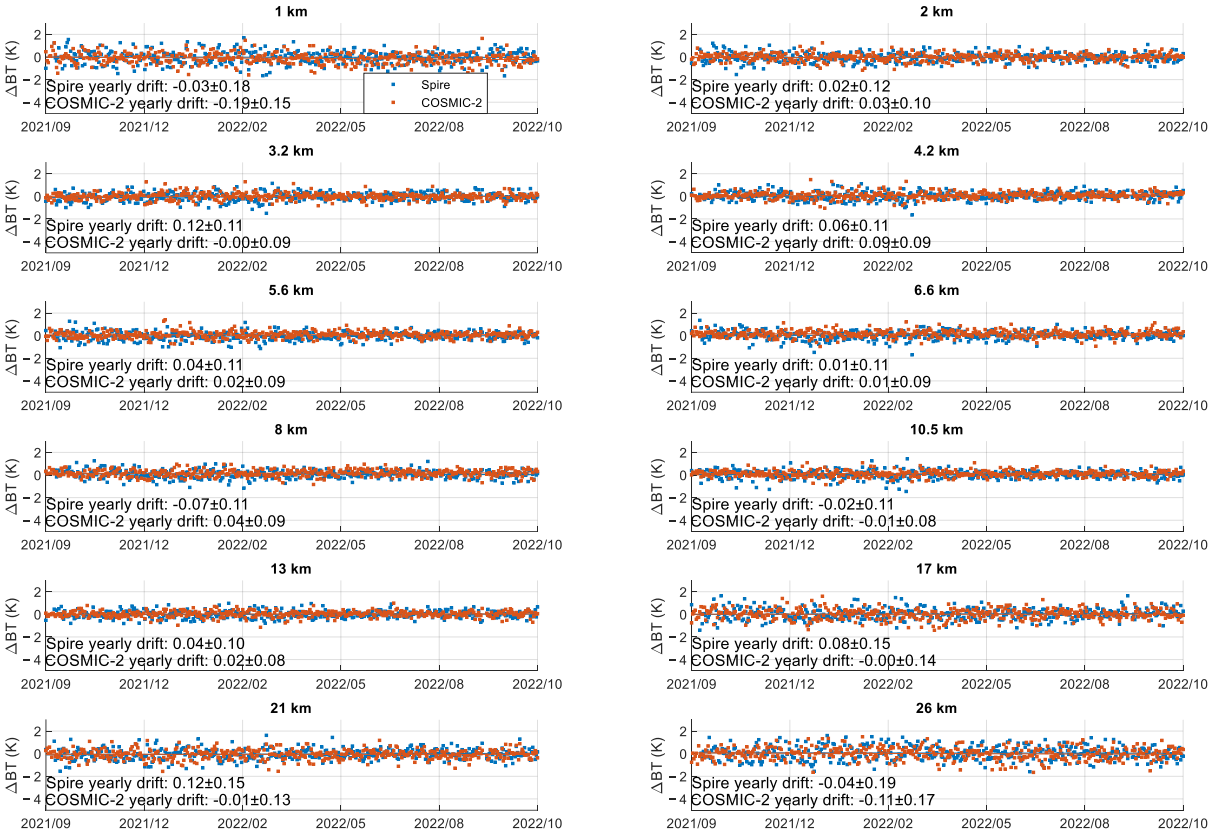

Figure 10. The time series and trend and its associated 95% confidence interval of daily T differences between Spire/COSMIC-2 and radiosonde measurements from 8 September 2021 and 31 October 2021 for 12 heights of interest.

In terms of the daily T difference trend $D(\Delta T_{RO\_raob})$, Table 3 shows that both $D\left(\Delta T_{Spire\_raob}\right)$ and $D(\Delta T_{C2\_raob})$ are within 0.19 K/year for all heights, except for the height of 30 km, where the yearly drift is relatively large and reaches -0.28 K/year. This larger drift is mainly due to larger T difference uncertainties and fewer profiles at this height. For example, Spire and COSMIC-2 have 1514 and 1542 profiles, respectively, as seen in Figure 8b. As for the yearly drift difference between Spire and COSMIC-2 $\Delta D\left(\Delta T_{Spire\_C2}\right)$, using the double difference method with RS41 radiosonde data as a transfer reference, the two RO temperature trends agree with each other within 0.16 K/year.

Considering the comparison with ATMS over ocean and radiosonde over land, the Spire and COSMIC-2 daily BT and T difference trends agree very well at different heights. Their BT and T differences through the double difference method are all within 0.16 K.

4.2. The Latitude Dependency Evaluation of BT Simulated with SPIRE and COSMIC-2 RO Soundings Using ATMS BT as a Reference

As mentioned in Section 3.1, COSMIC-2 RO events cover only latitudes within $\pm 45°$, while Spire observes at all latitudes. To eliminate the influence of different latitudinal coverages on the comparison results, only RO events from the same latitudinal region (45°S to 45°N) are included in Section 4.1. However, the impact of different latitudinal coverage on the results must also be evaluated to comprehensively analyze the performance of the two sets of RO data. Figure 11a shows the globally distributed difference between BT simulated using Spire and COSMIC-2 GNSS RO soundings, and BT observed for ATMS CH12. Meanwhile, Figure 11b reveals the difference between Spire and COSMIC-2 GNSS RO sounding T and radiosonde T at the height of 26 km. These figures are shown without latitude limitations. The BT difference distributions in Figure 11a show more Spire-ATMS collocations than COSMIC-2-ATMS collocations in the extensive ocean regions poleward of

±45° latitude. Therefore, it is reasonable to assume that $\mu(\Delta BT_{RO\_ATMS})$ with a latitude limitation may be quite different from $\mu(\Delta BT_{RO\_ATMS})$ without a latitude limitation. On the other hand, the maps of the geographical distribution of $\mu\left(\Delta T_{Spire\_raob}\right)$ and $\mu(\Delta T_{C2\_raob})$ are similar (Figure 11b), mainly because there are few radiosonde stations poleward of ±45° latitude. Therefore, only the latitude impacts on RO-based BT simulation and ATMS BT observation differences are evaluated.

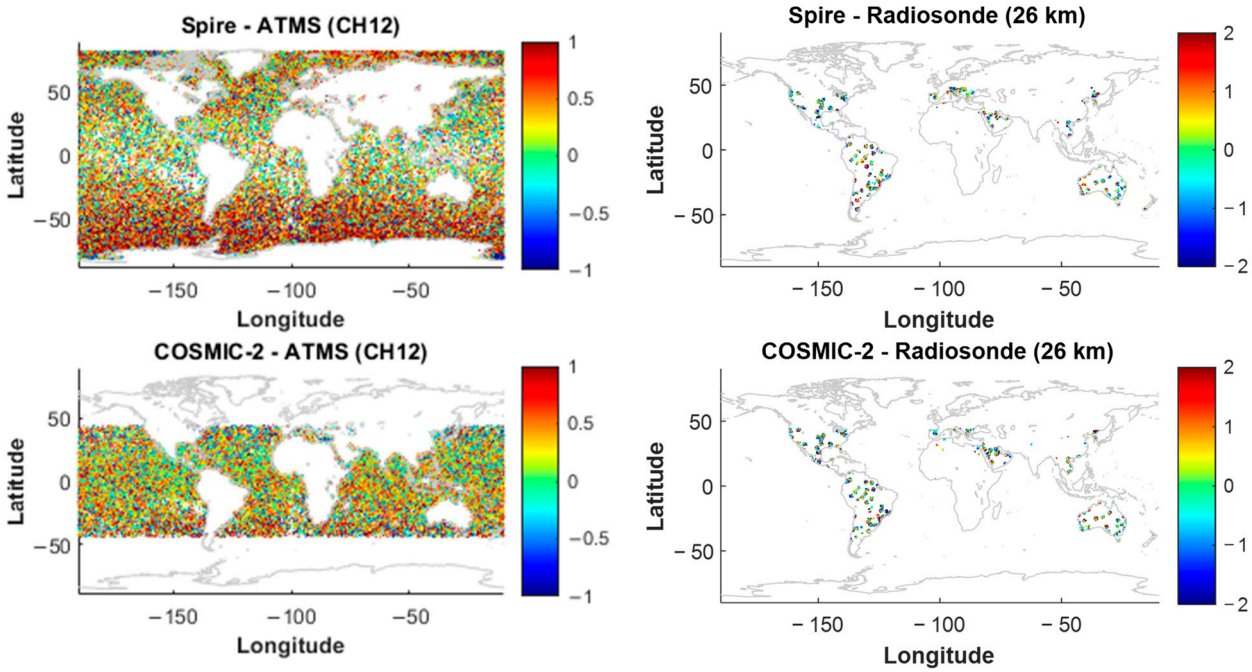

Figure 11. (**a**) The Spire (**top**)/COSMIC-2 (**bottom**) RO-simulated and ATMS-observed BT difference map for ATMS CH12 and (**b**) the Spire (**top**)/COSMIC-2 (**bottom**) RO and radiosonde T difference map at the height of 26 km. Note that these figures show data without any latitude limitations.

Table 4 lists the simulated BT differences between Spire and COSMIC-2—i.e., $\mu\left(\Delta BT_{Spire\_C2}\right)$ computed using the double difference method and ATMS BT as a transfer reference. This analysis is performed with and without latitude limitations. For comparison purposes, the results of applying a limited latitude in Table 2 are also included in Table 4. From the double difference result, $\mu\left(\Delta BT_{Spire\_C2}\right)$, it is obvious that by limiting latitude, the simulated BT differences in Spire and COSMIC-2 are more consistent with each other for most ATMS channels of interest, except CH19, whose peak sounding height is lower than 4 km. And the absolute BT differences in Spire and COSMIC-2 are comparable with or without latitude limitations for the ATMS CH10 and CH14. The value of $\mu\left(\Delta BT_{Spire\_C2}\right)$ without a latitude limitation reaches 0.37 K. This is much larger than the largest $\mu\left(\Delta BT_{Spire\_C2}\right)$ value found after applying a latitude limitation, which is 0.20 K for ATMS CH14 with the weighting function peak sounding height of 35.66 km.

Another important and interesting phenomenon from Figure 11a is the latitudinal dependence of the difference between BT simulated using Spire and COSMIC-2 GNSS RO soundings and BT observed for ATMS CH12. To study the latitude-dependent difference between CRTM-simulated BTs generated from Spire and COSMIC-2 soundings with respect to observed ATMS BT, the $\mu(\Delta BT_{RO\_ATMS})$ difference data were collected over the following five latitude regions: Antarctic (−90° to −45° latitude); Southern Hemisphere sub-tropics and mid-latitudes (−45° to −20° latitude); near-equator tropics (−20° to 20° latitude), Northern Hemisphere sub-tropics and mid-latitudes (20° to 45° latitude), and Arctic (45° to 90° latitude). Figure 12a,b show the mean differences and uncertainties

of ΔBT_{Spire_ATMS} and ΔBT_{C2_ATMS}, respectively, calculated over these five latitude regions with the data from 8 September 2021 to 31 October 2022. Since COSMIC-2 only covers the -45° to 45° latitude area, only three latitude regions have been plotted. Similar to Figure 7a, both the time series mean BT difference in $\mu(\Delta BT_{Spire\_ATMS})$ and $\mu(\Delta BT_{C2\_ATMS})$ and the BT difference uncertainty in $\sigma(\Delta BT_{Spire\_ATMS})$ and $\sigma(\Delta BT_{C2\_ATMS})$ are consistent in both the magnitude and sign for all ATMS channels of interest and all latitude regions.

Table 4. The simulated BT differences between Spire and COSMIC-2, with and without latitude limitations, computed using the double difference method and ATMS BT as a transfer reference.

RO vs. ATMS (Spire-COSMIC-2, K)		
Channel (Peak Sounding Height, km)	**Latitude Limited**	**Latitude Unlimited**
7 (8.06)	0.00	0.14
8 (10.61)	−0.01	−0.03
9 (13.08)	−0.04	−0.19
10 (17.10)	0.03	−0.02
11 (20.89)	0.07	0.15
12 (25.84)	0.04	0.15
13 (30.87)	−0.01	0.06
14 (35.66)	−0.05	0.04
19 (3.18)	0.12	0.03
20 (4.27)	0.14	0.16
21 (5.58)	0.17	0.26
22 (6.66)	0.20	0.37

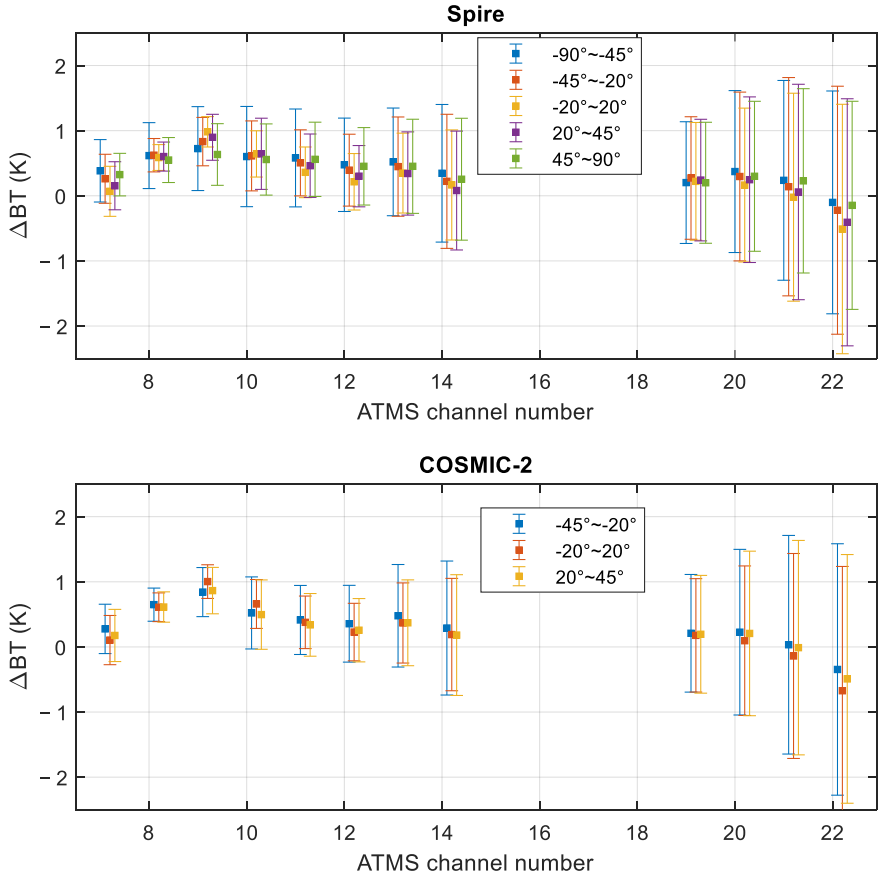

Figure 12. Latitude-dependence of the time series mean and standard deviation of BT differences between CRTM-simulated BT from Spire (**top**)/COSMIC-2 (**bottom**) soundings and observed BT from ATMS over five latitude regions for ATMS CH10–14 and CH19–22.

Regarding latitude dependency, in general, the simulated BTs generated with RO soundings are consistent with ATMS measurements over these five latitude regions within 0.4 K in $\mu(\Delta BT_{RO\_ATMS})$ for all ATMS channels of interest. For ATMS CH08, CH10, and CH19, the differences in $\mu(\Delta BT_{Spire\_ATMS})$ among these five latitude regions are within 0.10 K. However, for ATMS CH07, CH09, CH11-14, and CH20-22, the difference in $\mu(\Delta BT_{Spire\_ATMS})$ among five latitude regions is relatively larger (~0.2 K to ~0.4 K). Such remnant latitude-dependent differences can be seen in Figure 11a for ATMS CH12. For BTs simulated with COSMIC-2 RO soundings and observed by ATMS, the latitude dependency comparison in Figure 12b shows a similar magnitude and tendency to the latitude dependency comparison shown in Figure 12a for BTs simulated with Spire RO soundings and observed by ATMS in Figure 12a. However, since only three latitude regions need to be calculated, the BT differences among these three latitude regions are no larger than 0.33 K, which is relatively smaller than the BT differences for $\mu(\Delta BT_{Spire\_ATMS})$ among these five latitude regions. Therefore, BTs simulated using Spire and COSMIC-2 RO soundings show similar latitude dependencies relative to BTs observed by ATMS for the channels of interest in this study.

4.3. The Local Time Dependency Evaluation of BT Simulated with Spire and COSMIC-2 RO Soundings Using ATMS BT as a Reference

RO data may have diurnal cycle sampling errors. For example, if the diurnal temperature variation is large, local time (LT) intervals that do not account for the whole day may not reflect the actual temperature trend. This, in turn, introduces climatological errors [44–48]. For this reason, this paper also analyzes the local time distribution impact on the performance of CRTM-simulated BTs generated with Spire and COSMIC-2 RO soundings.

Figure 13 shows the one-day local time and latitude distributions of Spire and COSMIC-2 observations on 31 August 2022. COSMIC-2 occultation events have a relatively uniform local time coverage in each geographic coverage area equatorward of ±45° latitudes, while Spire exhibits a concentrated local time distribution.

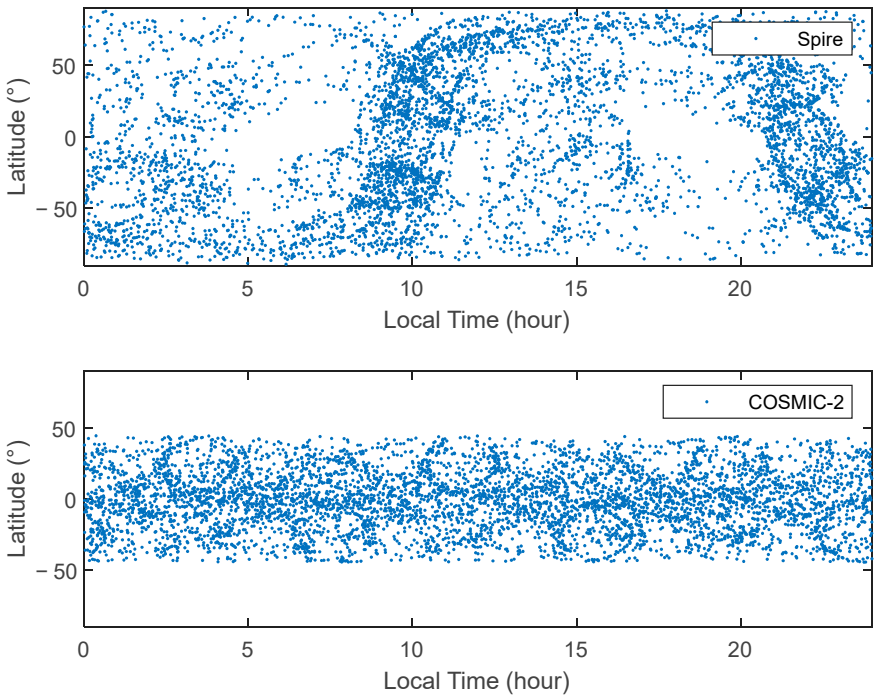

Figure 13. Local time–latitude distributions of collocated Spire/COSMIC-2 and ATMS measurements on 31 August 2022. The results for Spire and COSMIC-2 are found in the upper and lower panels, respectively.

Due to its various inclination orbits (51.6°, 83°/85°, and 37°), Spire sensors provide uneven local time coverage over the diurnal cycle; therefore, it is necessary to further investigate the impact of local time on the RO product's performance. Figure 14 shows the local time distributions of Spire and COSMIC-2 with and without latitude limitations from 8 September 2021 to 31 October 2022. The with/without latitude limitation condition has a very small impact on the local time coverage distribution. It can be seen that although Spire shows somewhat of a concentrated local time distribution in Figure 13, it still covers 24 h local time for latitude bands poleward of about ±20° latitudes. Note that although Figure 13a shows a gap in time coverage for Spire soundings in the tropics, the Spire soundings are globally covered throughout the study time interval of this paper. But at the same time, Figure 14 indicates that the local time of some Spire occultation events is concentrated at 0900–1200 and 2100–2300. However, COSMIC-2 observations are equally distributed at the local time around the globe and provide uniform local time coverage.

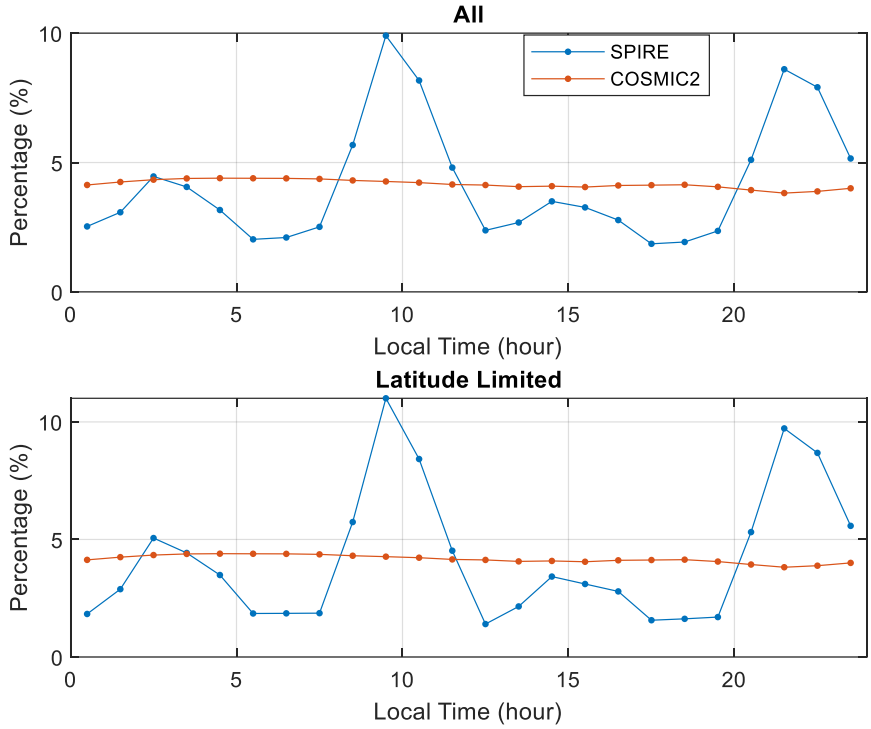

Figure 14. Local time distributions for Spire and COSMIC-2 soundings with and without latitude limitations from 8 September 2021 to 31 October 2022.

Figure 15 shows the local time-dependence of the time series mean of Spire/COSMIC-2 RO CRTM-simulated BT and ATMS BT difference ($\mu(\Delta BT_{Spire\_ATMS})$ and $\mu(\Delta BT_{C2\_ATMS})$) for selected ATMS channels: CH08 (peak sounding height 10.61 km), CH12 (peak sounding height 25.84 km), and CH20 (peak sounding height 4.27 km), with limiting Spire latitude to ±45°. The values of $\mu(\Delta BT_{RO\_ATMS})$ have been binned into 1-hour groups in the figure. It is shown that the values of $\mu(\Delta BT_{Spire\_ATMS})$ and $\mu(\Delta BT_{C2\_ATMS})$ as a function of local time are stable and consistent for ATMS CH08, are relatively stable but show some differences for ATMS CH12, and are somewhat unstable and show relatively large differences for ATMS CH20. For other ATMS channels of interest in this work—e.g., CH7, CH09-10, CH13-14, CH19, and CH21-22—$\mu(\Delta BT_{RO\_ATMS})$ local time-dependency for Spire and COSMIC-2 are very similar (not shown here). The results indicate that although the local time geographical distributions of Spire and COSMIC-2 show different patterns, the local time-based performance is comparable. Note that since there are not enough numbers matching pairs between RO and radiosonde to be binned into different local time groups, the values of $\mu(\Delta T_{RO\_RAOB})$ are not used to investigate local time dependency.

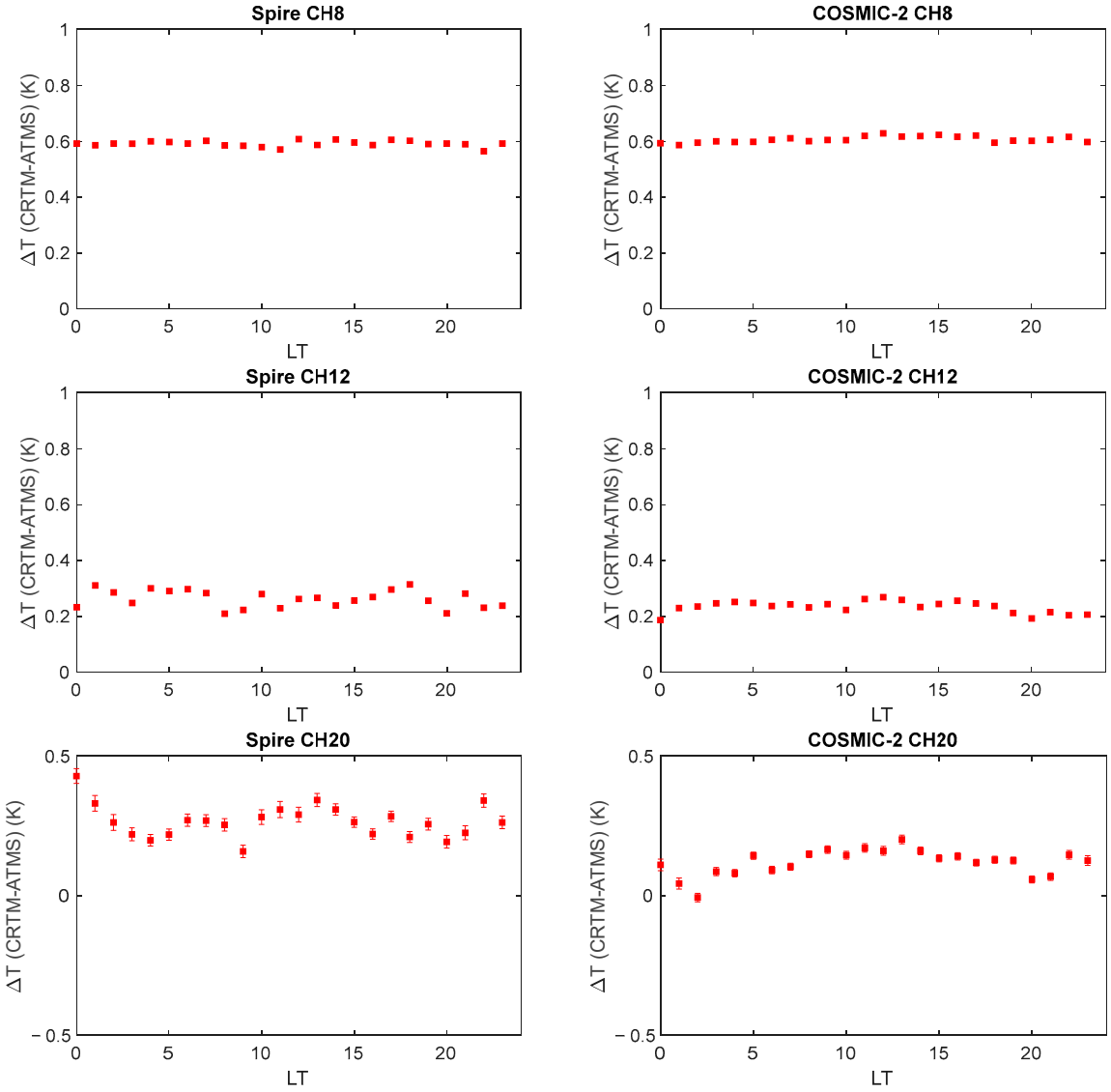

Figure 15. Local time-dependence of the time series mean of Spire/COSMIC-2 RO CRTM-simulated BT and ATMS BT differences ($\mu\left(\Delta BT_{Spire\_ATMS}\right)$ and $\mu(\Delta BT_{C2\_ATMS})$) for ATMS CH08, CH12, and CH20 and Spire soundings limited to within $\pm 45^{\circ}$ latitude.

4.4. The SNR-Related Dependency Evaluation of BT Simulated with Spire and COSMIC-2 RO Soundings Using ATMS BT as a Reference

For GNSS RO instruments, the signal-to-noise ratio (SNR) is the RO signal amplitude divided by the noise level and is provided in the voltage-to-voltage unit (V/V). The GNSS RO SNR includes transmitted RO signal noise contributions and GNSS LEO satellite noise contributions—e.g., signal ray path and RO receiver noise. The SNR parameter is crucial for assessing RO performance. Previous studies indicate that higher SNR has advantages in studying the troposphere and the Planetary Boundary Layer (PBL) [49, 50], which is expected to improve retrieval quality. The COSMIC-2 RO receivers have higher SNR values than any previous RO missions, owing to the advanced Tri-Global Navigation Satellite System Radio Occultation Receiver (TGRS) and high-gain antenna [51]. As Sokolovskiy et al. [52] and Schreiner et al. [51] pointed out, high SNR is most important for providing deep signals in the tropical troposphere. Higher SNR is also important for detecting sharp PBL tops. Therefore, quantitative characterization of the advantages of high SNR for RO instruments is an important issue. On this basis, we analyzed the influence of SNR on the bending angle lapse (BAL) and penetration depth. Different

missions significantly differ in the nominal values of SNR. The normalized values may have a smaller difference due to different noise floors [53]. Therefore, to compare RO missions with different SNR values, the influence of SNR on the comparison of CRTM-simulated BT based on Spire/COMSIC-2 soundings with respect to ATMS BT products was also analyzed.

The ability to penetrate low altitudes is one of the decisive factors linked to the efficiency of RO-based inversions of important weather parameters in the lower troposphere. For this reason, a parameter named "penetration depth" exists that defines the minimum altitude above ground level with a valid bending angle for an occultation event. An analysis of occultation event penetration depths as a function of altitude was performed. Figure 16 shows the distributions of the penetration depths for all latitude-limited Spire and COSMIC-2 data. It can be seen that the two cumulative curves do not precisely overlap. Still, they can be considered almost identical, indicating that the two ROs have almost the same ability to penetrate the atmosphere.

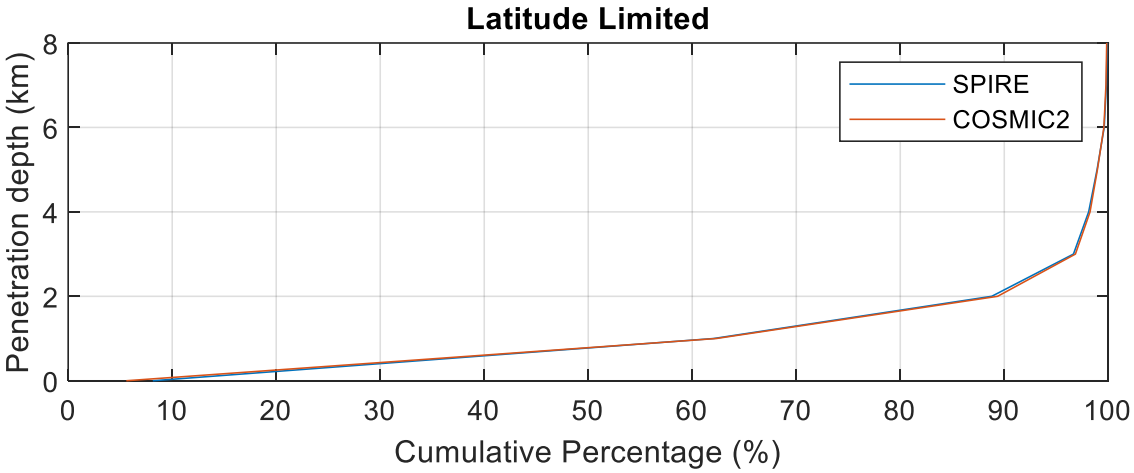

Figure 16. Distributions of the penetration depths (minimum heights above ground level) for Spire and COSMIC-2 soundings limited within ±45° latitude.

Figure 17 shows the average penetration depth versus the L1 signal-to-noise ratio for Spire (solid blue line) and COSMIC-2 (blue dashed line) for an interval of 50 V/V, with RO data limited to ±45° latitude. The COSMIC-2 L1 SNR can reach as large as 2500 V/V, and Spire reaches ~2200 V/V. The plot comparing SNR and penetration depth demonstrates that a higher SNR allows lower altitude penetration. It can be seen that the Spire and COSMIC-2 have similar performance in detecting low-altitude areas at SNR less than 1900 V/V. But for SNR values greater than 1900 V/V, Spire penetration depth detection shows unstable performance instead of having deeper penetration like COSMIC-2. The penetration depth indicates the low-altitude penetration capability of RO systems, while BAL can be applied by utilizing its maximum value to detect the top of the PBL [48]. Therefore, Figure 17 also indicates Spire (solid orange line) and COSMIC-2 (dashed orange line) BAL as a function of L1 SNR for RO data limited within ±45° latitude. Sharp PBL tops can be detected at the heights of maximum BAL [54]. Higher SNR allows retrievals of bending angle profiles with larger BAL, thus increasing the reliability of detection of sharp PBL tops. The BAL of COSMIC-2 gradually increased with increasing SNR. The trend of Spire BAL with SNR is almost the same as COSMIC-2, out of which the Spire BAL shows an unstable performance when the SNR reaches about 1900 V/V. This is because when the SNR exceeds 1900 V/V, Spire's data volume rapidly decreases to no more than 350, while COSMIC-2's data volume remains around 40,000. Therefore, the performance of BAL and the penetration depth of Spire are similar to that of COSMIC-2, with the interval of the SNR less than 1900 V/V for RO data limited within ±45° latitude.

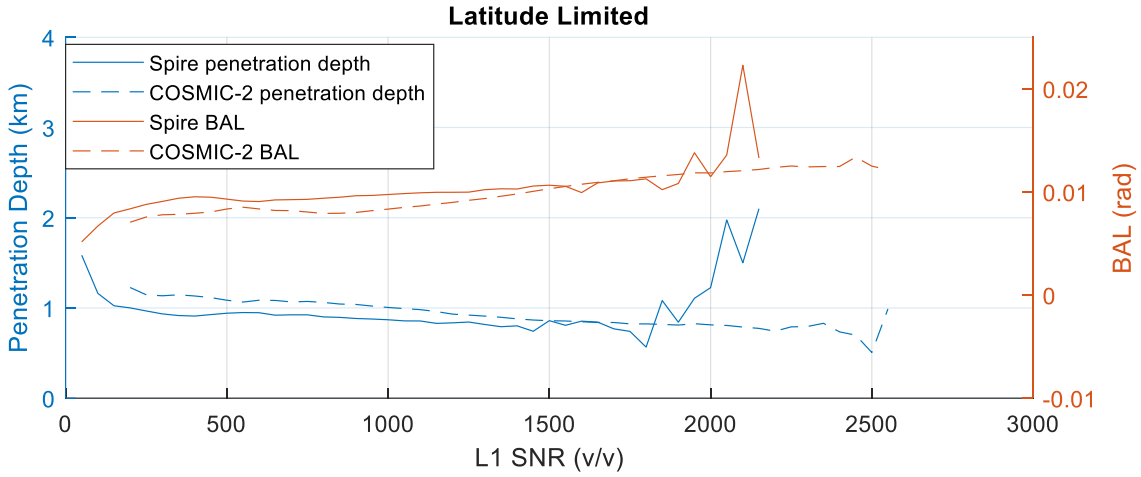

Figure 17. Spire and COSMIC-2 penetration depths and BAL as a function of L1 SNR for RO soundings limited within ±45° latitude.

As mentioned above, since different RO missions have different nominal SNR values, this paper analyzes the SNR-based performance of the two RO missions by comparing Spire/COSMIC-2-based CRTM-simulated BT with ATMS-observed BT at different SNR levels. This was carried out in addition to the previous comparisons between the SNR of Spire and COSMIC-2. Figure 18 shows the $\mu(\Delta BT_{Spire\_ATMS})$ and $\mu(\Delta BT_{C2\_ATMS})$ over three SNR levels of 0–1000 (V/V), 1000–2000 (V/V), and 2000–3000 (V/V). Note that the Spire and ATMS collocations do not contain data points with the SNR larger than 2000 V/V, so there is no $\mu(\Delta BT_{Spire\_ATMS})$ value for the 2000~3000 V/V category plotted in Figure 18. For $\mu(\Delta BT_{Spire\_ATMS})$ and $\mu(\Delta BT_{C2\_ATMS})$ at the available SNR categories, Figure 18 shows that there are almost no differences compared with the $\mu(\Delta BT_{Spire\_ATMS})$ and $\mu(\Delta BT_{C2\_ATMS})$ values given in Figure 7a,b and Table 2. This indicates that the SNR magnitude does not impact $\mu(\Delta BT_{RO\_ATMS})$. The main discrepancies between $\mu(\Delta BT_{Spire\_ATMS})$ and $\mu(\Delta BT_{C2\_ATMS})$ at the three SNR levels are in ATMS CH19-22. This is most likely due to the larger uncertainty of these channels and the sensitivity of the retrieval algorithm to tropospheric moisture at a height below 8 km. Overall, these results demonstrate that despite Spire having a lower SNR than that of COSMIC-2, it exhibited comparable (but not outperforming) performance to COSMIC-2 compared with ATMS observations, indicating that lower SNR missions, such as Spire, can also provide good inversion results. And this conclusion is consistent with previous work presented in [55–58].

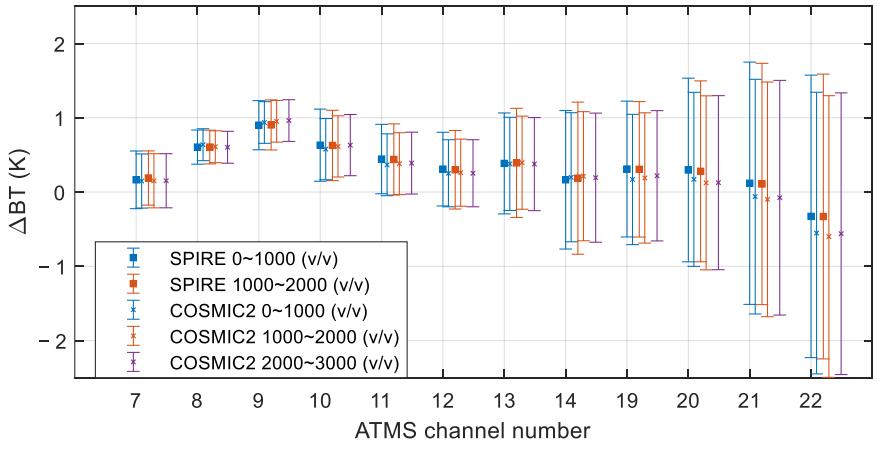

Figure 18. Mean BT differences (K) of Spire/COSMIC-2-based CRTM-simulated BT and ATMS-observed BT over three SNR range categories: 0–1000 (V/V), 1000–2000 (V/V), and 2000–3000 (V/V).

5. Conclusions

This study evaluated the performance of the Spire RO instrument by comparing its data with that from COSMIC-2. This was carried out to clarify the performance consistency of its temperature products with respect to existing high-precision RO products and their applicability to accurate numerical weather forecasting. Spire, a commercial manufacturer of the Spire RO sensor, has continued to augment the temporal and spatial coverage of RO data since 2021. In addition, the COSMIC-2/FORMOSAT-7 constellation with six satellites has produced RO data since 2019. The availability of large and growing datasets from multiple RO missions and historical data provides a unique opportunity to establish long-term Climate Data Records (CDRs) grade global temperature, water vapor, and derived climatology data products. By combining multi-mission RO data with radiosonde data and microwave remote sensing data, scientists can better understand the Earth's atmosphere and how it changes over time. This information can be used to improve weather forecasting, climate modeling, and our understanding of the impacts of climate change on the Earth's ecosystems and human populations. Consistent temperature and water vapor data processing are essential to ensure that the resulting datasets are high quality and suitable for climate studies. By comparing the Spire RO data with other RO missions, microwave data, and radiosonde data, our work can help validate the RO data's quality and ensure it is suitable for climate studies. In addition, demonstrating the consistency of RO data from different receivers and RO signals is an important step toward establishing the usefulness and reliability of the RO technique for climate studies and other applications. It also helps to ensure that the resulting datasets are International System of Units (SI) traceable, meaning they can be traced back to the SI standards maintained by the global network of national standards laboratories that are internationally recognized and standardized.

To achieve this purpose, the NOAA-20 ATMS microwave brightness temperature (BT) product and radiosonde RS41 temperature measurements were used as benchmarks over ocean and land, respectively. The CRTM-simulated BTs and retrieved atmospheric T profiles from Spire and COSMIC-2 RO soundings were compared separately with NOAA-20 ATMS observed BTs and radiosonde RS41 temperature measurements, respectively, for the period 7 September 2021 to 31 October 2022. These data were used to compute statistics of the BT (T) differences and their trends to evaluate the stability and consistency between Spire/COSMIC-2 RO mission data and the benchmark instrument data over ocean and land. The inter-sensor Spire and COSMIC-2 BT (T) differences were derived with the double difference method using the ATMS BT (radiosonde T) as a transfer reference. The ATMS CH07-CH14 and CH19-CH22 measurements, whose peak weighting function heights range from 3.18 km to 35.66 km and radiosonde height from 0.2 km to 30 km, were used for the evaluation.

This study analyzed Spire measurement quality and data coverage capabilities considering the following three mission characteristics. Firstly, COSMIC-2 LEO satellite orbital inclination is 24°, which limits its RO sounding data over a range of 45°N to 45°S. Spire sensors, on the other hand, are placed in LEO with varying inclinations, which provides the sensor constellation with global coverage. Secondly, Spire sensors provide unevenly distributed 24 h local time coverage, whereas COSMIC-2 sensors are equally distributed in local time around the Earth and provide RO data with uniform local time coverage. Given that the local time distribution impacts the climatological sampling error of RO, an analysis of the consistency of Spire and COSMIC-2 based on local time was performed. Third, a great advantage of COSMIC-2 is that signal-to-noise ratio values are higher than any previous RO mission, achieved by its advanced TGRS system and high-gain antenna. Previous studies indicate that SNR impacts at least three aspects of RO performance: studying the Planetary Boundary Layer, detecting deep signals in the tropical troposphere, and detecting sharp atmospheric boundary layer tops. Therefore, to comprehensively understand the performance consistency of Spire and COSMIC-2, not only the overall BT and T difference and their trends are estimated using ATMS and radiosonde data as references, but also the

consistency of Spire and COSMIC-2 based on different latitude intervals, different local times, as well as SNR range categories are evaluated through ATMS.

The main conclusions are summarized as follows.

i. The time series statistics and trends of the differences in Spire/COSMIC-2 CRTM-simulated BT (sounding profile T) and ATMS-observed BT (radiosonde profile T) over the ocean (land).

The results show that both the time series mean difference between CRTM-simulated BT from Spire/COSMIC-2 RO data and ATMS-observed BT over the ocean, $\mu(\Delta BT_{Spire\_ATMS})$ and $\mu(\Delta BT_{C2\_ATMS})$, and BT difference uncertainty, $\sigma(\Delta BT_{Spire\_ATMS})$ and $\sigma(\Delta BT_{C2\_ATMS})$, are consistent in the magnitude for all ATMS channels of interest. The values of $\mu(\Delta BT_{Spire\_ATMS})$ and $\mu(\Delta BT_{C2\_ATMS})$ are all within 1 K. The Spire and COSMIC-2 BT difference, computed with the double difference method using ATMS BT observations as a transfer reference, $\mu(\Delta BT_{Spire\_C2})$, are within 0.07 K for ATMS CH07-14 with peak heights from 8–36 km and within 0.20 K for ATMS CH19-22 with peak heights from 3–7 km. In terms of the mean difference between Spire/COSMIC-2 RO sounding profile T and radiosonde RS41 profile T over land, both time series mean difference, $\mu(\Delta T_{RO\_raob})$, and uncertainty, $\sigma(\Delta T_{RO\_raob})$, are consistent in both the magnitude and sign for all heights of interest. The values of $\mu\left(\Delta T_{Spire\_raob}\right)$ and $\mu(\Delta T_{C2\_raob})$ are within 0.17 K for all heights except 0.2 km, where the difference reaches to 0.41 K and 0.24 K for Spire and COSMIC-2, respectively. For Spire and COSMIC-2, the T difference using the radiosonde profile T as a transfer reference, $\mu(\Delta T_{Spire\_C2})$, is within 0.17 K for all heights. Generally, Spire and COSMIC-2 show good consistency over the ocean and land.

ii. The trend comparison of the difference in Spire/COSMIC-2 CRTM-simulated BT (sounding profile T) and ATMS-observed BT (radiosonde profile T) over the ocean (land).

(1) The discrepancy of the difference trends in the first two months for ATMS CH12-14 shows that COSMIC-2 and Spire RO data captured the UCAR WetPf2 1D-Var algorithm updates, i.e., Spire and COSMIC-2 change to ECMWF 6 h forecasts as a priori values around 27 October 2022 and on 28 September 2021, respectively, very well. The difference between ATMS BT and CRTM-simulated BT using COSMIC-2 and Spire soundings is improved for ATMS CH12-14 after the update.

(2) The daily BT difference yearly trends between Spire CRTM-simulated BT and ATMS-observed BT, $D(\Delta BT_{Spire\_ATMS})$, over the ocean, is no larger than 0.07 K/year for all ATMS channels of interest except for ATMS CH14, which is -0.08 K/year. Similarly, the values of $D(\Delta BT_{C2\_ATMS})$ are no larger than 0.11 K/year for all ATMS channels of interest. The Spire and COSMIC-2 BT difference trend comparison computed using ATMS-observed BT as a transfer reference, $D(\Delta BT_{Spire\_C2})$, is within 0.07 K/year except for ATMS CH14, which is -0.12 K/year. This is due to the background assimilation change in Spire data in the first two months of the period studied in this paper, which results in a noticeable jump in Spire data. And although COSMIC-2 also experienced a background data update on 8 September 2021, it did not show up because its update happened to be outside of the study period of this paper. The trend shows that in terms of sounding profile T difference, yearly drift between RO and radiosonde, $D(\Delta T_{RO\_RAOB})$, over land, have larger scattering and uncertainty compared with their BT counterparts. The values of $D(\Delta T_{RO\_RAOB})$ are no larger than 0.12 K/year at all heights except $D(\Delta T_{C2\_RAOB})$ at 0.2 km, 1 km, and 30 km. The larger drift is mainly due to much fewer data points. The drifts between Spire and COSMIC-2 sounding profile T, using radiosonde sounding profile T as a transfer reference, $D(\Delta T_{Spire\_C2})$, is within 0.13 K/year except for the heights of 0.2 km and 1.0 km, which reach 0.16 K/year. Overall, Spire and COSMIC-2 BT and the T difference yearly drift over ocean and land show good consistency. They agree with each other within 0.16 K/year.

iii. The BT latitude dependency evaluation of Spire and COSMIC-2 through ATMS and radiosonde over ocean and land, respectively.

(1) We evaluated the overall BT (T) differences between Spire and COSMIC-2 with and without latitude limitations, using the double difference method by ATMS (radiosonde). The results show that after applying a latitude limitation, the $\mu(\Delta BT_{Spire\_ATMS})$ and $\mu(\Delta BT_{C2\_ATMS})$ are more consistent with each other for most ATMS channels in general, which is because the number of collocations between RO and ATMS accounts for a large percentage outside $\pm 45^{\circ}$. On the other hand, $\mu\left(\Delta T_{Spire\_raob}\right)$ and $\mu(\Delta T_{C2\_raob})$ are comparable, with or without latitude limitations, due to the fact that a majority of the collocation between RO and radiosonde are within $\pm 45^{\circ}$.

(2) The $\mu(\Delta BT_{Spire\_ATMS})$ and $\mu(\Delta BT_{C2\_ATMS})$ at different latitude regions over ocean are also evaluated. Generally, the simulated Spire and COSMIC-2 BT are consistent with ATMS measurements over all different latitude regions, indicating that Spire and COSMIC-2 have similar temperature performance at different latitude regions, and the two RO sensors show similar latitude dependency for ATMS CH08 and CH13-14.

iv. The BT local time dependency evaluation of Spire and COSMIC-2 through ATMS over the ocean.

(1) Spire sensors have various inclination orbits (51.6°, 83°/85°, and 37°), and they provide an inconsistent local time coverage over the full 24 h diurnal cycle, while COSMIC-2 occultation events have relatively even local time coverage over the diurnal cycle within $\pm 45^{\circ}$ latitude.

(2) Local time dependence of $\mu(\Delta BT_{Spire\_ATMS})$ and $\mu(\Delta BT_{C2\_ATMS})$ for ATMS channels was evaluated by binning the local time into 1-hour groups. The results show that although the difference between $\mu(\Delta BT_{Spire\_ATMS})$ and $\mu(\Delta BT_{C2\_ATMS})$ for different ATMS channels may vary, the local time-based performance is stable and similar for the two RO mission products for all ATMS channels of interest. However, as mentioned above, Spire and COSMIC-2 RO data have different local time geographical distribution patterns.

v. The BT SNR-related dependency evaluation of Spire and COSMIC-2 through ATMS over the ocean.

(1) SNR-related penetration depth and bending angle lapse of Spire and COSMIC-2 were evaluated. After limiting Spire latitude, the distributions of the penetration depths for Spire and COSMIC-2 were almost identical, and the performances of BAL were similar. However, COSMIC-2 had a higher SNR than Spire over the same latitude range.

(2) The SNR-based performance of the two RO sensors was also analyzed by comparing CRTM-simulated BT and ATMS-observed BT at different SNR levels. The Spire BT difference was higher than the COSMIC-2 BT difference for ATMS CH19-CH22 overall SNR levels. Still, no obvious dependence of BT differences as a function of SNR was identified for COSMIC-2 and Spire from the results, indicating that the SNR-based performances of the two RO sensors are comparable, although COSMIC-2 had a higher SNR than Spire and more stable performance at high SNR values.

This study confirms that the Spire RO nanosatellites produce high-quality RO measurements. With global coverage, Spire RO data can complement the COSMIC-2 coverage restricted to low-latitude regions. The local time coverage evaluation results suggest that future Spire satellite constellations would benefit by being designed to achieve a more evenly distributed local time coverage. The analysis of the impact of SNR-related parameters on RO performance shows that, despite Spire having lower SNR values than COSMIC-2, it has measurements that can penetrate effectively into the lower troposphere, detect PBL height, and retrieve high-quality temperature estimates. Our results indicate that Spire can yield high-quality RO data comparable to the COSMIC-2 mission. Long-term environmental monitoring with multi-ROs is possible if Spire data are continuously acquired and processed consistently.

Author Contributions: Conceptualization, X.J., S.-P.H. and X.S.; methodology, X.J., S.-P.H. and X.S.; software, X.J. and T.-C.L.; validation, X.J., S.-P.H., X.S., T.-C.L., Y.C. and X.Z.; formal analysis, X.J., S.-P.H. and X.S.; investigation, X.J., S.-P.H., X.S. and Y.C.; resources, S.-P.H., X.S. and Y.C.; data

curation, X.J.; writing—original draft preparation, X.J.; writing—review and editing, X.J., S.-P.H., X.S., T.-C.L., Y.C. and X.Z.; visualization, X.J.; supervision, S.-P.H. and X.S.; project administration, S.-P.H. and X.S.; funding acquisition, S.-P.H. and X.S. All authors have read and agreed to the published version of the manuscript.

Funding: This study was supported by NOAA grant NA19NES4320002 (Cooperative Institute for Satellite Earth System Studies—CISESS) at the University of Maryland/ESSIC.

Data Availability Statement: The data presented in this study are available on request from the corresponding author.

Acknowledgments: The authors would like to thank Bin Zhang and Loknath Adhikari for their input during the development of this manuscript.

Conflicts of Interest: The authors declare no conflict of interest.

References

1. Kuo, Y.-H.; Wee, T.-K.; Sokolovskiy, S.; Rocken, C.; Schreiner, W.; Hunt, D.; Anthes, R. Inversion and Error Estimation of GPS Radio Occultation Data. *J. Meteorol. Soc. Jpn. Ser. II* **2004**, *82*, 507–531. [CrossRef]
2. Ho, S.-P.; Goldberg, M.; Kuo, Y.-H.; Zou, C.-Z.; Shiau, W. Calibration of Temperature in the Lower Stratosphere from Microwave Measurements Using COSMIC Radio Occultation Data: Preliminary Results. *Terr. Atmos. Ocean. Sci.* **2009**, *20*, 87. [CrossRef]
3. Yunck, T.P.; Liu, C.-H.; Ware, R. A History of GPS Sounding. *Terr. Atmos. Ocean. Sci.* **2000**, *11*, 001. [CrossRef]
4. Hajj, G.A.; Lee, L.C.; Pi, X.; Romans, L.J.; Schreiner, W.S.; Straus, P.R.; Wang, C. COSMIC GPS Ionospheric Sensing and Space Weather. *Terr. Atmos. Ocean. Sci.* **2000**, *11*, 235–272. [CrossRef]
5. Kursinski, E.R.; Hajj, G.A.; Bertiger, W.I.; Leroy, S.S.; Meehan, T.K.; Romans, L.J.; Schofield, J.T.; McCleese, D.J.; Melbourne, W.G.; Thornton, C.L.; et al. Initial Results of Radio Occultation Observations of Earth's Atmosphere Using the Global Positioning System. *Science* **1996**, *271*, 1107–1110. [CrossRef]
6. Wang, B.-R.; Liu, X.-Y.; Wang, J.-K. Assessment of COSMIC radio occultation retrieval product using global radiosonde data. *Atmos. Meas. Tech.* **2013**, *6*, 1073–1083. [CrossRef]
7. Anthes, R.A.; Bernhardt, P.A.; Chen, Y.; Cucurull, L.; Dymond, K.F.; Ector, D.; Healy, S.B.; Ho, S.-P.; Hunt, D.C.; Kuo, Y.; et al. The COSMIC/FORMOSAT-3 Mission: Early Results. *Bull. Am. Meteorol. Soc.* **2008**, *89*, 313–334. [CrossRef]
8. Ho, S.-P.; Kirchengast, G.; Leroy, S.; Wickert, J.; Mannucci, A.J.; Steiner, A.; Hunt, D.; Schreiner, W.; Sokolovskiy, S.; Ao, C.; et al. Estimating the uncertainty of using GPS radio occultation data for climate monitoring: Intercomparison of CHAMP refractivity climate records from 2002 to 2006 from different data centers. *J. Geophys. Res. Atmos.* **2009**, *114*, D23107. [CrossRef]
9. Ho, S.-P.; Hunt, D.; Steiner, A.K.; Mannucci, A.J.; Kirchengast, G.; Gleisner, H.; Heise, S.; von Engeln, A.; Marquardt, C.; Sokolovskiy, S.; et al. Reproducibility of GPS radio occultation data for climate monitoring: Profile-to-profile inter-comparison of CHAMP climate records 2002 to 2008 from six data centers. *J. Geophys. Res. Atmos.* **2012**, *117*, D18111. [CrossRef]
10. Jing, X.; Shao, X.; Liu, T.-C.; Zhang, B. Comparison of GRUAN RS92 and RS41 Radiosonde Temperature Biases. *Atmosphere* **2021**, *12*, 857. [CrossRef]
11. Zhang, B.; Ho, S.-P.; Cao, C.; Shao, X.; Dong, J.; Chen, Y. Verification and Validation of the COSMIC-2 Excess Phase and Bending Angle Algorithms for Data Quality Assurance at STAR. *Remote Sens.* **2022**, *14*, 3288. [CrossRef]
12. Ho, S.-P.; Zhou, X.; Shao, X.; Chen, Y.; Jing, X.; Miller, W. Assessment of Spire Data in the Neutral Atmosphere. *Remote Sens.* **2023**. *submitted*.
13. Ho, S.-P.; Kireev, S.; Shao, X.; Zhou, X.; Jing, X. Processing and Validation of the STAR COSMIC-2 Temperature and Water Vapor Profiles in the Neutral Atmosphere. *Remote Sens.* **2022**, *14*, 5588. [CrossRef]
14. Cao, C.; Wang, W.; Lynch, E.; Bai, Y.; Ho, S.-P.; Zhang, B. Simultaneous Radio Occultation for Intersatellite Comparison of Bending Angles toward More Accurate Atmospheric Sounding. *J. Atmos. Ocean. Technol.* **2020**, *37*, 2307–2320. [CrossRef]
15. Li, Y.; Kirchengast, G.; Scherllin-Pirscher, B.; Schwaerz, M.; Nielsen, J.K.; Ho, S.-P.; Yuan, Y.-B. A New Algorithm for the Retrieval of Atmospheric Profiles from GNSS Radio Occultation Data in Moist Air and Comparison to 1DVar Retrievals. *Remote Sens.* **2019**, *11*, 2729. [CrossRef]
16. Shao, X.; Ho, S.-P.; Zhang, B.; Cao, C.; Chen, Y. Consistency and Stability of SNPP ATMS Microwave Observations and COSMIC-2 Radio Occultation over Oceans. *Remote Sens.* **2021**, *13*, 3754. [CrossRef]
17. Chen, Y.; Cao, C.; Shao, X.; Ho, S.-P. Assessment of the Consistency and Stability of CrIS Infrared Observations Using COSMIC-2 Radio Occultation Data over Ocean. *Remote Sens.* **2022**, *14*, 2721. [CrossRef]
18. Ho, S.-P.; Pedatella, N.; Foelsche, U.; Healy, S.; Weiss, J.-P.; Ullman, R. Using Radio Occultation Data for Atmospheric Numerical Weather Prediction, Climate Sciences, and Ionospheric Studies and Initial Results from COSMIC-2, Commercial RO Data, and Recent RO Missions. *Bull. Am. Meteorol. Soc.* **2022**, *103*, E2506–E2512. [CrossRef]
19. Shao, X.; Ho, S.P.; Jing, X.; Zhou, X.; Chen, Y.; Liu, T.C.; Zhang, B.; Dong, J. Characterizing the Tropospheric Water Vapor Variation using COSMIC Radio Occultation and ECMWF Reanalysis Data. *Atmos. Chem. Phys. Discuss.* **2023**. *preprint*. [CrossRef]

20. Irisov, V.; Masters, D.; Gorbunov, M.; Nguyen, V.; Sikarin, R.; Bloom, A.; Rocken, C. Comparison of Spire RO profiles processed by UCAR and Spire. In Proceedings of the 8th International Radio Occultation Working Group Meeting—IROWG-8, Virtual, 7–13 April 2021.
21. McCarty, W.; Todling, R.; Privé, N.; Chattopadhyay, M.; Partyka, G.; Gelaro, R. Assessment of New Radio Occultation Measurements at the Global Modeling and Assimilation Office. In Proceedings of the 8th International Radio Occultation Working Group Meeting—IROWG-8, Virtual, 7–13 April 2021.
22. Murphy, M.J.; Haase, J.S. Evaluation of GNSS Radio Occultation Profiles in the Vicinity of Atmospheric Rivers. *Atmosphere* **2022**, *13*, 1495. [CrossRef]
23. Angling, M.J.; Nogués-Correig, O.; Nguyen, V.; Vetra-Carvalho, S.; Bocquet, F.-X.; Nordstrom, K.; Melville, S.E.; Savastano, G.; Mohanty, S.; Masters, D. Sensing the ionosphere with the Spire radio occultation constellation. *J. Space Weather Space Clim.* **2021**, *11*, 56. [CrossRef]
24. Bosch, G. GNSS Radio Occultation in Advanced Numerical Weather Prediction Models. *GEOmedia* **2019**, *23*, 34–37. [CrossRef]
25. Forsythe, V.V.; Duly, T.; Hampton, D.; Nguyen, V. Validation of Ionospheric Electron Density Measurements Derived from Spire CubeSat Constellation. *Radio Sci.* **2020**, *55*, e2019RS006953. [CrossRef]
26. Zeng, Z.; Schreiner, W.S.; Weiss, J. Evaluation of Spire GNSS RO data for global tropopause and PBL detections. *AGU Fall Meet. Abstr.* **2020**, *2020*, IN029-02.
27. Alessandro, P. *SPIRE/STRATOS (GNSS-RO) Quality Assessment Summary*; Telespazio: Rome, Italy, 2020.
28. Ho, S.-P.; Zhou, X.; Kuo, Y.-H.; Hunt, D.; Wang, J.-H. Global Evaluation of Radiosonde Water Vapor Systematic Biases using GPS Radio Occultation from COSMIC and ECMWF Analysis. *Remote Sens.* **2010**, *2*, 1320–1330. [CrossRef]
29. Sun, B.; Reale, A.; Seidel, D.J.; Hunt, D.C. Comparing radiosonde and COSMIC atmospheric profile data to quantify differences among radiosonde types and the effects of imperfect collocation on comparison statistics. *J. Geophys. Res. Atmos.* **2010**, *115*, D23104. [CrossRef]
30. He, W.; Ho, S.-P.; Chen, H.; Zhou, X.; Hunt, D.; Kuo, Y.-H. Assessment of radiosonde temperature measurements in the upper troposphere and lower stratosphere using COSMIC radio occultation data. *Geophys. Res. Lett.* **2009**, *36*, L17807. [CrossRef]
31. Shao, X.; Ho, S.-P.; Zhang, B.; Zhou, X.; Kireev, S.; Chen, Y.; Cao, C. Comparison of COSMIC-2 radio occultation retrievals with RS41 and RS92 radiosonde humidity and temperature measurements. *Terr. Atmos. Ocean. Sci.* **2021**, *32*, 1015–1032. [CrossRef]
32. Ho, S.-P.; Anthes, R.A.; Ao, C.O.; Healy, S.; Horanyi, A.; Hunt, D.; Mannucci, A.J.; Pedatella, N.; Randel, W.J.; Simmons, A.; et al. The COSMIC/FORMOSAT-3 Radio Occultation Mission after 12 Years: Accomplishments, Remaining Challenges, and Potential Impacts of COSMIC-2. *Bull. Am. Meteorol. Soc.* **2020**, *101*, E1107–E1136. [CrossRef]
33. Veenus, V.; Das, S.S.; Sama, B.; Uma, K.N. A comparison of temperature and relative humidity measurements derived from COSMIC-2 radio occultations with radiosonde observations made over the Asian summer monsoon region. *Remote Sens. Lett.* **2022**, *13*, 394–405. [CrossRef]
34. Ho, S.-P.; Zhou, X.; Shao, X.; Zhang, B.; Adhikari, L.; Kireev, S.; He, Y.; Yoe, J.G.; Xia-Serafino, W.; Lynch, E. Initial Assessment of the COSMIC-2/FORMOSAT-7 Neutral Atmosphere Data Quality in NESDIS/STAR Using In Situ and Satellite Data. *Remote Sens.* **2020**, *12*, 4099. [CrossRef]
35. Kim, E.; Abraham, S.; Amato, J.; Blackwell, W.J.; Cho, P.; Fuentes, J.; Hernquist, M.; Kam, J.; Leslie, R.V.; Liu, Q.; et al. An Evaluation of NOAA-20 ATMS Instrument Pre-Launch and On-Orbit Performance Characterization. *IEEE Trans. Geosci. Remote Sens.* **2022**, *60*, 5302813. [CrossRef]
36. Iacovazzi, R.; Lin, L.; Sun, N.; Liu, Q. NOAA Operational Microwave Sounding Radiometer Data Quality Monitoring and Anomaly Assessment Using COSMIC GNSS Radio-Occultation Soundings. *Remote Sens.* **2020**, *12*, 828. [CrossRef]
37. Kishore, P.; Ratnam, M.V.; Namboothiri, S.; Velicogna, I.; Basha, G.; Jiang, J.; Igarashi, K.; Rao, S.; Sivakumar, V. Global (50°S–50°N) distribution of water vapor observed by COSMIC GPS RO: Comparison with GPS radiosonde, NCEP, ERA-Interim, and JRA-25 reanalysis data sets. *J. Atmos. Sol.-Terr. Phys.* **2011**, *73*, 1849–1860. [CrossRef]
38. Jauhiainen, H.; Lentonen, J.; Survo, P.; Lehtinen, R.; Pietari, T. The implications of Vaisala's new radiosonde RS41 on improved in-situ observations for meteorological applications. In Proceedings of the AMS Annual Meeting 2014, Atlanta, GA, USA, 2–6 February 2014.
39. Han, Y. *JCSDA Community Radiative Transfer Model (CRTM): Version 1*; NOAA: Washington, DC, USA, 2006.
40. Liu, Q.; Yan, B.; Garrett, K.; Ma, Y.; Liang, X.; Huang, J.; Wang, W.; Cao, C. Deriving Surface Reflectance from Visible/Near Infrared and Ultraviolet Satellite Observations through the Community Radiative Transfer Model. *IEEE J. Sel. Top. Appl. Earth Obs. Remote Sens.* **2022**, *15*, 2004–2011. [CrossRef]
41. Gelaro, R.; Johnson, B.T. The Community Radiative Transfer Model (CRTM): Recent Improvements and Applications. In Proceedings of the 103rd AMS Annual Meeting, Denver, CO, USA, 8–12 January 2023.
42. Steiner, A.K.; Lackner, B.C.; Ladstädter, F.; Scherllin-Pirscher, B.; Foelsche, U.; Kirchengast, G. GPS radio occultation for climate monitoring and change detection. *Radio Sci.* **2011**, *46*, RS0D24. [CrossRef]
43. Kursinski, E.R.; Hajj, G.A.; Schofield, J.T.; Linfield, R.P.; Hardy, K.R. Observing Earth's atmosphere with radio occultation measurements using the Global Positioning System. *J. Geophys. Res. Atmos.* **1997**, *102*, 23.429–23.465. [CrossRef]
44. Foelsche, U.; Borsche, M.; Steiner, A.K.; Gobiet, A.; Pirscher, B.; Kirchengast, G.; Wickert, J.; Schmidt, T. Observing upper troposphere–lower stratosphere climate with radio occultation data from the CHAMP satellite. *Clim. Dyn.* **2008**, *31*, 49–65. [CrossRef]

45. Pirscher, B.; Foelsche, U.; Lackner, B.C.; Kirchengast, G. Local time influence in single-satellite radio occultation climatologies from Sun-synchronous and non-Sun-synchronous satellites. *J. Geophys. Res. Atmos.* **2007**, *112*, D1119. [CrossRef]
46. Shen, Z.; Zhang, K.; He, Q.; Wan, M.; Li, L.; Wu, S. Quest over the Sampling Error of COSMIC Radio Occultation Temperature Climatologies. *J. Atmos. Ocean. Technol.* **2021**, *38*, 441–458. [CrossRef]
47. Kirk-Davidoff, D.B.; Goody, R.M.; Anderson, J.G. Analysis of Sampling Errors for Climate Monitoring Satellites. *J. Clim.* **2005**, *18*, 810–822. [CrossRef]
48. Chang, H.; Lee, J.; Yoon, H.; Morton, Y.J.; Saltman, A. Performance assessment of radio occultation data from GeoOptics by comparing with COSMIC data. *Earth, Planets Space* **2022**, *74*, 108. [CrossRef]
49. Sokolovskiy, S.; Schreiner, W.; Zeng, Z.; Hunt, D.; Lin, Y.-C.; Kuo, Y.-H. Observation, analysis, and modeling of deep radio occultation signals: Effects of tropospheric ducts and interfering signals. *Radio Sci.* **2014**, *49*, 954–970. [CrossRef]
50. Sokolovskiy, S.; Rocken, C.; Hunt, D.; Schreiner, W.; Johnson, J.; Masters, D.; Esterhuizen, S. GPS profiling of the lower troposphere from space: Inversion and demodulation of the open-loop radio occultation signals. *Geophys. Res. Lett.* **2006**, *33*, L14816. [CrossRef]
51. Schreiner, W.S.; Weiss, J.P.; Anthes, R.A.; Braun, J.; Chu, V.; Fong, J.; Hunt, D.; Kuo, Y.-H.; Meehan, T.; Serafino, W.; et al. COSMIC-2 Radio Occultation Constellation: First Results. *Geophys. Res. Lett.* **2020**, *47*, e2019GL086841. [CrossRef]
52. Sokolovskiy, S.; Schreiner, W.; Weiss, J.; Zeng, Z.; Hunt, D.; Braun, J. Initial assessment of COSMIC-2 data in the lower troposphere (LT). In Proceedings of the Joint 6th ROM SAF User Workshop and 7th IROWG Workshop 2019, Elsinore, Denmark, 19–25 September 2019.
53. Gorbunov, M.; Irisov, V.; Rocken, C. Noise Floor and Signal-to-Noise Ratio of Radio Occultation Observations: A Cross-Mission Statistical Comparison. *Remote Sens.* **2022**, *14*, 691. [CrossRef]
54. Sokolovskiy, S.V.; Rocken, C.; Lenschow, D.H.; Kuo, Y.-H.; Anthes, R.A.; Schreiner, W.S.; Hunt, D.C. Observing the moist troposphere with radio occultation signals from COSMIC. *Geophys. Res. Lett.* **2007**, *34*, L18802. [CrossRef]
55. Irisov, V.; Duly, T.; Nguyen, V.; Masters, D.; Nogues-Correig, O.; Tan, L.; Yuasa, T.; Ector, D.R. Recent radio occultation profile results obtained from Spire's CubeSat GNSS-RO constellation. *AGU Fall Meet. Abstr.* **2018**, *2018*, A44G-04.
56. Irisov, V.; Ector, D.; Duly, T.; Nguyen, V.; Nogues-Correig, O.; Tan, L.; Yuasa, T. Atmospheric Radio Occultation Observation from Spire CubeSat Nanosatellites. In Proceedings of the 98th American Meteorological Society Annual Meeting, Austin, TX, USA, 7–11 January 2018.
57. Irisov, V.; Nguyen, V.; Duly, T.; Nogués-Correig, O.; Tan, L.; Yuasa, T.; Ringer, J.; Masters, D.; Sikarin, R.; Gorbunov, M.; et al. Radio Occultation Observations and Processing from Spire's CubeSat Constellation. In Proceedings of the Joint 6th ROM SAF User Workshop and 7th IROWG Workshop, EUMETSAT ROM SAF, Elsinore, Denmark, 19–25 September 2019.
58. Bowler, N.E. An assessment of GNSS radio occultation data produced by Spire. *Q. J. R. Meteorol. Soc.* **2020**, *146*, 3772–3788. [CrossRef]